HHS Public Access

Author manuscript

Neuroimage. Author manuscript; available in PMC 2021 August 01.

Published in final edited form as:

Neuroimage. 2021 August 01; 236: 118042. doi:10.1016/j.neuroimage.2021.118042.

Asymmetric neural dynamics characterize loss and recovery of consciousness☆

Zirui Huang[a,b,*], **Vijay Tarnal**[a,b], **Phillip E. Vlisides**[a,b], **Ellen L. Janke**[a,b], **Amy M. McKinney**[a], **Paul Picton**[a], **George A. Mashour**[a,b,c], **Anthony G. Hudetz**[a,b,c,*]

[a]Department of Anesthesiology, University of Michigan Medical School, Ann Arbor, MI 48109, USA

[b]Center for Consciousness Science, University of Michigan Medical School, Ann Arbor, MI 48109, USA

[c]Neuroscience Graduate Program, University of Michigan, Ann Arbor, MI 48109, USA

Abstract

Anesthetics are known to disrupt neural interactions in cortical and subcortical brain circuits. While the effect of anesthetic drugs on consciousness is reversible, the neural mechanism mediating induction and recovery may be different. Insight into these distinct mechanisms can be gained from a systematic comparison of neural dynamics during slow induction of and emergence from anesthesia. To this end, we used functional magnetic resonance imaging (fMRI) data obtained in healthy volunteers before, during, and after the administration of propofol at incrementally adjusted target concentrations. We analyzed functional connectivity of corticocortical and subcorticocortical networks and the temporal autocorrelation of fMRI signal as an index of neural processing timescales. We found that *en route* to unconsciousness, temporal autocorrelation across the entire brain gradually increased, whereas functional connectivity gradually decreased. In contrast, regaining consciousness was associated with an abrupt restoration

☆Original data and code that support the findings of this study are available from the corresponding authors (Z.H. and A.G.H.) upon reasonable request.

*Corresponding authors. huangzu@umich.edu (Z. Huang), ahudetz@med.umich.edu (A.G. Hudetz). .

Author contributions

Z.H. designed and conducted the experiments, analyzed the data, interpreted data, and wrote the article; V.T., P.E.V., E.L.J., and P.P. performed the anesthetic procedures; A.M.M. coordinated the experiment. G.A.M. interpreted data and wrote the article; A.G.H. conceived and supervised the project, designed the experiment, interpreted data, and wrote the article.

Credit author statement

Zirui Huang: Conceptualization, Methodology, Software, Formal analysis, Investigation, Data Curation, Writing - Original Draft, Writing - Review & Editing, Visualization

Vijay Tarnal: Investigation

Phillip E. Vlisides: Investigation

Ellen L. Janke: Investigation

Amy M. McKinney: Project administration

Paul Picton: Investigation

George A. Mashour: Writing - Original Draft, Writing - Review & Editing, Supervision

Anthony G. Hudetz: Conceptualization, Methodology, Investigation, Writing - Original Draft, Writing - Review & Editing, Supervision, Funding acquisition

Declaration of Interests

The authors declare no competing interests.

Supplementary materials

Supplementary material associated with this article can be found, in the online version, at doi:10.1016/j.neuroimage.2021.118042.

of cortical but not subcortical temporal autocorrelation and an abrupt boost of subcorticocortical functional connectivity. Pharmacokinetic effects could not account for the difference in neural dynamics between induction and emergence. We conclude that the induction and recovery phases of anesthesia follow asymmetric neural dynamics. A rapid increase in the speed of cortical neural processing and subcorticocortical neural interactions may be a mechanism that reboots consciousness.

Keywords

Anesthetic hysteresis; Consciousness; Functional connectivity; Neural inertia; fMRI

Introduction

Research with noninvasive neuroimaging in humans and primates reveals that anesthetic-induced unconsciousness is associated with an extensive disruption of neural activity and functional connectivity of large-scale brain networks (Barttfeld et al., 2015; Bonhomme et al., 2016; Boveroux et al., 2010; Demertzi et al., 2019; Huang et al., 2020; Tanabe et al., 2020). Disruptions of corticocortical and subcorticocortical neuronal interactions likely contribute to loss of consciousness by preventing the integration of bottom-up and top-down data streams (Aru et al., 2020; Mashour and Hudetz, 2018, 2017), a proposition also supported by mechanistic studies at cellular level (Halassa et al., 2014; Hudetz et al., 2020; Redinbaugh et al., 2020; Suzuki and Larkum, 2020).

Most former studies implicitly assumed a unitary relationship between the level of consciousness and the applied dose of a specific anesthetic. The process of emergence from anesthesia has been historically treated as a passive process, depicted as the inverse or “mirror image” of induction (McKay et al., 2006). However, empirical observations and theoretical modeling have suggested that induction and emergence phases may be asymmetric. This asymmetry is manifested in a phenomenon called anesthetic hysteresis (Steyn-Ross et al., 2004). Namely, when comparing the behavioral changes during increasing vs. decreasing anesthetic concentration in preclinical experiments, the induction of unconsciousness required a higher anesthetic concentration than that required to maintain unconsciousness during the recovery phase. As a result, the graphical relationship between a suitable measure of arousal or level of consciousness and the anesthetic dose encloses a hysteresis loop (Friedman et al., 2010; Joiner et al., 2013). Such hysteresis has been demonstrated with various anesthetic agents in various species from mammals to insects. Traditionally, this asymmetry has been attributed to a pharmacokinetic effect but experimental and theoretical work in the past decade supports the alternative hypothesis that such an asymmetry is driven by distinct neural dynamics (Proekt and Hudson, 2018; Proekt and Kelz, 2020). The tendency to maintain unconsciousness at a lower dose than that required to induce unconsciousness has been described as “neural inertia,” an intrinsic neuronal resistance to behavioral state transitions (Friedman et al., 2010; Joiner et al., 2013).

In spite of the clear preclinical evidence, anesthetic hysteresis (and neural inertia) in humans has been controversial (Breshears et al., 2010; Ferreira et al., 2020; Kuizenga et al., 2018;

Lewis et al., 2018; Proekt and Kelz, 2018; Pullon et al., 2020; Purdon et al., 2013; Sepúlveda et al., 2019; Warnaby et al., 2017) suggesting a need for further investigations. Other than studies employing multichannel EEG or ECoG (Breshears et al., 2010; Lewis et al., 2018; Pullon et al., 2020; Purdon et al., 2013; Warnaby et al., 2017), there has been no human neuroimaging, such as functional magnetic resonance imaging (fMRI), investigation of the question. Although the temporal resolution of fMRI lags behind that of the EEG or local neuronal signals, fMRI still provides sufficient temporal grain to detect a potential difference in the dynamics of regional brain activation or functional connectivity and could be instrumental in further testing the hypothesis of anesthetic hysteresis. Moreover, the spatiotemporal redistribution of activity and connectivity of brain networks during the bidirectional transitions into and out of unconsciousness could illuminate the potential mechanism of neural inertia at a systems level. Understanding the mechanism of neural inertia would have both basic and translational scientific importance. Scientifically, it would provide insight into adaptive neuronal phenomena. Clinically, it could help establish novel therapeutic targets to selectively stabilize or destabilize the anesthetized state, which could inform therapeutic interventions in patients with disorders of consciousness.

To examine the above questions, we aimed to compare the time courses of fMRI-based neural activity in healthy volunteers before, during, and after the administration of propofol at incrementally adjusted target concentrations. We hypothesized that assessing time-dependent measures of neural processing would reveal asymmetric neural dynamics consistent with anesthetic hysteresis across bidirectional transitions of the state of consciousness. We analyzed the dynamic functional connectivity of cortical and subcortical networks as well as the temporal autocorrelation of the fMRI signal that characterizes the speed (timescale) of neural processing. To achieve a coherent understanding across multiple spatial scales, we assessed the fMRI-derived quantities at regional, specific network, and global (whole brain) levels. We report that differential changes in specific corticocortical and subcorticocortical network dynamics during slow induction and emergence indeed occur, consistent with anesthetic hysteresis. Furthermore, we demonstrate that this hysteresis cannot be accounted for solely by pharmacokinetics, supporting the hypothesis of an intrinsic neural inertia that impedes the return of consciousness in human participants.

Materials and methods

Participants in pharmacological setting

The experimental protocol was previously described and part of the imaging data were published in a different context (Huang et al., 2018b). The University of Michigan Institutional Review Board (IRB) approved the experimental protocol. All methods were performed in accordance with the relevant guidelines and regulations. Following careful discussion and written informed consent, twenty-six healthy participants (right-handed; ages between 19–34 years old; 13 females) were recruited. All participants were classified as American Society of Anesthesiologists physical status 1. Subjects were excluded from participation if they had any contraindication to MRI scanning, possible pregnancy, extreme obesity, metallic substances in the body, claustrophobia, anxiety, or cardiopulmonary disease; had a history of neurological, cardiovascular, or pulmonary illness; significant head

injury with loss of consciousness; learning disability or other developmental disorder; sleep apnea or any severe snoring history; sensory/motor loss sufficient to interfere with performance of the study, gastroesophageal reflux disease; unwilling to abstain from alcohol use for 24 h prior to their scheduled MRI study visit; had a history of drug use or a positive drug screen; had tattoos on the head or neck region; had a history of allergic reaction to eggs; had an intracranial structural abnormality on T1-weighted MRI scans or experienced physical discomfort during fMRI scanning.

Anesthetic agents

Propofol was our reference drug, which has been the most widely used agent in human fMRI studies of anesthetic effects (Adapa et al., 2014; Boveroux et al., 2010; Davis et al., 2007; Dueck et al., 2005; Gross et al., 2019; Huang et al., 2018b; Huang et al., 2016; Lichtner et al., 2018; Liu et al., 2012; Mhuircheartaigh et al., 2010; Schroter et al., 2012; Warnaby et al., 2016). The advantage of propofol is that it exerts minimal effects on cerebral hemodynamics (Fiset et al., 1999; Kondo et al., 2016) and can be carefully titrated. Because it preserves flow-metabolism coupling in the cerebral vasculature, it minimizes confound of the fMRI interpretation. Propofol suppresses neuronal activity mainly through an enhancement of GABA-A receptor-mediated inhibition thus modulating widespread targets throughout the brain (Alkire et al., 2008).

Anesthetic administration and monitoring

All subjects fasted for 8 h before the study. On the day of the experiment, an attending anesthesiologist completed a pre-operative assessment and physical examination. Two fully trained anesthesiologists were physically present for the entire duration of the experiment. An intravenous cannula was placed after a subcutaneous injection of lidocaine (0.5 ml of 1%) used as local anesthetic. Spontaneous respiration, end-tidal CO_2, heart rate, pulse oximetry, and electrocardiogram were continuously monitored during the experiment. Noninvasive arterial pressure was measured with MR-compatible automatic monitor. Supplemental oxygen (2 L/min via nasal cannula) was used for all subjects. The propofol administration was achieved by target-controlled IV bolus and constant rate infusion. The bolus dose, infusion rate and infusion duration for each target effect-site concentration (ESC) and for each participant were pre-determined based on a pharmacokinetic model (Marsh et al., 1991) developed for target-controlled propofol infusion and implemented in software (STANPUMP Shafer (1996)). The dosing (bolus + infusion) was incremented at every 5 min until the final target was reached. The incremental dosing (0.4 μg/ml) was used to titrate the anesthetic level to the point of loss of behavioral responsiveness (LOR). The initial target ESC was 0.4 μg/ml in 14 participants and 1.0 μg/ml in 12 participants. The final target concentration was 2.4 μg/ml (in 6 participants from our previous study (Huang et al., 2018b)) or one increment above that first resulted in LOR (in 20 participants). The final target was maintained for 21.6 min on average (±SD = 10.2 min). After that, the infusion was terminated to allow spontaneous emergence. The estimated ESC time course for each participant was calculated after completing the experiment by taking account of the individual differences in the infusion timing, rate and duration.

Experimental task during fMRI

Behavioral responsiveness was assessed by motor response (squeezing a rubber ball by hand), which defined the periods during which a participant retained responsiveness (PreLOR), loss of responsiveness (LOR) before spontaneous emergence, prior to recovery of responsiveness during emergence (PreROR), and recovery of responsiveness (ROR). Two 10 min resting-state baseline and two 15 min task baseline recordings were done before (Rest1 and Base1) and after (Base2 and Rest2) propofol infusion (Fig. 1A). There were 60 motor response trials distributed throughout the entire scan, with an inter-trial-interval of ~90 s. The beginning of trial was cued with the spoken word “action”, following which the participants were required to grip the rubber ball once (instructed before the experiment). Between the motor response trials, participants were instructed to perform mental imagery tasks (playing tennis, spatial navigation and squeeze imagery). A pseudo-randomized (Latin square) block design was applied, in which 15 s periods of tennis (and navigation) imagery, and 10 s periods of squeeze imagery with a hand squeeze within 5 s after hearing the instruction, alternated with 15 s of rest. The entire scan included 180 rest–imagery cycles (60 cycles per condition). See our previous publication for more details about mental imagery tasks (Huang et al., 2018b). The beginning of each mental imagery trial was cued with the spoken word “tennis imagery,” “navigation imagery,” “squeeze imagery,” and the rest period was cued with the word “relax.” The verbal instructions were programmed using E-Prime 3.0 (Psychology Software Tools, Pittsburgh, PA) and delivered via an audiovisual stimulus presentation system designed for an MRI environment. The volume of the headphones was adjusted for subject comfort. Behavioral responses were measured in mmHg of air pressure during squeezing the rubber ball, using BIOPAC (https://www.biopac.com) MP160 system with AcqKnowledge software (V5.0).

fMRI data acquisition

Data were acquired at University of Michigan Hospital using a 3T Philips scanner with a standard 32-channel transmit/receive head coil. Before fMRI scans, T1 weighted spoiled gradient recalled echo (SPGR) images was acquired for high spatial resolution of anatomical images with parameters: 170 sagittal slices, 1.0 mm thickness (no gap), TR = 8.1 s, TE = 3.7 ms, flip angle = 8°, FOV = 24 cm, image matrix 256×256. Functional images over the whole brain were acquired by a gradient-echo EPI pulse sequence with parameters: 28 slices, TR/TE = 800/25ms by multiband acquisition, MB factor = 4, slice thickness = 4 mm, in-plane resolution = 3.4 × 3.4 mm; field of view (FOV) = 220 mm, flip angle = 76°, image matrix: 64×64. Six participants were scanned with slightly different parameters before MRI hardware upgradation (21 slices, slice thickness = 6 mm, MB factor = 3). All participants were asked to lay at rest with eyes closed in the scanner for the first 10 min (Rest1) and the last 10 min (Rest2) resting-state scan. They were asked not to move and to stay awake. Verbal instructions were presented through earphones. Four task fMRI runs were conducted including 15 min wakeful baseline (Base1), during (30-min) and after (30 min) propofol infusion, and another 15 min recovery baseline (Base2). One participant lost behavioral responsiveness after the first 30 min fMRI run, and five participants regained behavioral responsiveness after the second 30 min fMRI run; the state transition time points for these participant was not recorded. In addition, one participants’ ROR data were shorter than the minimal requirement (at least 2 min data length) for the following sliding window analysis,

and one participant did not complete the study due to excessive body movement during ROR. In sum, our results were based on 18 optimal data from 26 studied subjects; those data captured reliable transition periods for both LOR and ROR.

fMRI data preprocessing

Preprocessing steps were implemented in AFNI (http://afni.nimh.nih.gov/afni). 1) Slice timing correction; 2) Rigid head motion correction/realignment within and across runs; frame-wise displacement (FD) of head motion was calculated using frame-wise Euclidean Norm (square root of the sum squares) of the six-dimension motion derivatives; 3) Coregistration with high-resolution anatomical images; 4) Spatial normalization into Talaraich stereotactic space and resampling to $3 \times 3 \times 3$ mm^3; 5) Using AFNI's function 3dTproject, the time-censored data were band-pass filtered to 0.008–0.25 Hz. At the same time, various undesired components (e.g., physiological estimates, motion parameters) were removed via linear regression. The undesired components included linear and nonlinear drift (polynomials up to and including degree 2), time series of head motion and its temporal derivative, and mean time series from the white matter and cerebrospinal fluid; 6) Spatial smoothing with 6 mm full-width at half-maximum isotropic Gaussian kernel; 7) The time-course per voxel of each run was normalized to zero mean and unit variance, accounting for differences in variance of non-neural origin (e.g., distance from head coil). For methodological considerations (Murphy and Fox, 2017), we performed the analyses both with and without global signal regression (GSR) and compared them in the Supplementary material. As temporal autocorrelation concerns local dynamics (see below), controlling shared signal across the whole brain (global signal) could presumably be beneficial for extracting the genuine local effect. Therefore, for the main results in this article, temporal autocorrelation was calculated after applying the GSR procedure while measures otherwise (functional connectivity measures; see below) were not.

Temporal autocorrelation

The timescale of fMRI signals was estimated for each voxel as the temporal autocorrelation decay (Huang et al., 2018a), quantified as the area under the curve (AUC) of the autocorrelation function from 0.8 to 12 s (0.8 s step, given TR = 0.8 s) including 15 correlation coefficients (Fig. 1B). The time window of 12 seconds was chosen in accordance with a previous study (Raut et al., 2020). We also varied the window length, ranging from 0.8 to 40 s, and evaluated the robustness of the results. The AUC is hereafter referred to as the autocorrelation index, where a higher value indicates a shift toward slower dynamics.

Strength centrality

The average fMRI time series across all voxels in the gray matter was extracted and defined as global signal. We computed Pearson's correlations between the global signal and the signal of each voxel in the gray matter. This yielded a whole-brain voxel-wise correlation map with a correlation coefficient (Fischer's Z transformed) per voxel (Fig. 1B). The value for each voxel is akin to a measure of unthresholded weighted degree centrality, which indexes the strength to which the signal of a given voxel is temporally coordinated with all other voxels' signal in the gray matter. In this study, we referred to it as strength centrality. The gray matter average of strength centrality was previously defined as global signal

functional connectivity (Tanabe et al., 2020), representing a net strength of whole brain activity coordination.

Definition of functional networks and brain atlas

We adopted a well-established network template (Power et al., 2011) that had been slightly modified in our previous study (Huang et al., 2018a). It contained 10 functional networks (226 functional areas in total): subcortical (SUB), dorsal attention (DA), ventral attention (VA), default mode (DMN), fronto-parietal task control (FPTC), cingulo-opercular task control (COTC), salience (SAL), sensory/somatomotor (SS), auditory (AUD), and visual networks (VIS). In addition, we adopted a brain region template using automated anatomical labeling (AAL) atlas (Tzourio-Mazoyer et al., 2002), containing 45 anatomical volumes of interest in each hemisphere. The above network and brain region templates were used to quantify the temporal autocorrelation and functional connectivity at both network and regional levels. We sought to take advantage from both templates, where the former included a reliable network definition (i.e., highly reproducible across studies), and the latter included a detailed regional parcellation across cortical and subcortical brain areas.

Within- and between-network functional connectivity

A functional connectivity matrix was generated by calculating the Pearson's correlation coefficient of the time courses between each pair of functional areas based on the aforementioned network template. This yielded a pairwise 226 × 226 correlation matrix (Fisher's Z transformed) per data unit (e.g., 2 min data in the following sliding window analysis). Within- or between-network functional connectivity was derived by computing the average of the triangular or rectangle zones of the matrix corresponding to a given network (within-network) or a pair of networks (between-network) (Fig. 1B).

Corticocortical and subcorticocortical functional connectivity

Similar to the above calculation of strength centrality, the average fMRI time series across all voxels in the cortex (instead of the entire gray-matter) was extracted. Pearson correlations between the cortical signal and the signal of each voxel in the gray matter were computed. This yielded a whole-brain voxel-wise correlation map with a correlation coefficient (Fischer's Z transformed) per voxel. The average of correlation coefficients across the cortex was defined as corticocortical functional connectivity. The above procedure was applied by using the average fMRI time series across voxels in a given subcortical region (e.g., thalamus or pallidum), yielding subcortical signal correlation maps. The average of correlation coefficients across a subcortical region in the cortical signal correlation map and the average of correlation coefficients across the cortex in a given subcortical correlation map was averaged again and defined as subcorticocortical (e.g., thalamocortical or pallidocortical) functional connectivity. The cortex mask was the cortical regions' union in the AAL atlas, and the subcortical masks were derived from the AAL atlas.

Sliding window analysis

The focus of this study was to delineate the state transitions as a function of drug effect, we adopted a sliding window approach in ESC, and the above fMRI measurements including

autocorrelation index, functional connectivity (strength centrality, within-network, between-network, corticocortical and subcorticocortical). One concern with the sliding window approach is the choice of window size, as it has been varied from tens of seconds to several minutes in previous practices (Barttfeld et al., 2015; Hindriks et al., 2016; Hutchison et al., 2013; Laumann et al., 2017; Tagliazucchi et al., 2016). Smaller window size may capture more transient changes of the dynamics but it can reduce the statistical reliability and make it more difficult to perform group averaging of dynamic time courses (Hindriks et al., 2016). On the other hand, longer window size may capture changes that are more static with larger statistical reliability, but with the cost of losing transient information. We traded off this issue by choosing a moderate window size with 2 min length (150 fMRI frames; linear trend was removed per window) and 20 s time step (25 fMRI frames). To this end, the sliding window time-courses are presumably reflect the dynamic changes induced by the anesthetics, instead of intrinsic variabilities. It thus permitted us to average the time-course of a given measurement across subjects. Given the data length of PreLOR, LOR, PreROR and ROR varied across participants, we used the transition points of LOR and ROR as two reference time points in order to align all participants' data within the same timeline. The sliding window was moving forward and backward centered at the reference time points, with a maximum data length of 15 min in each time direction.

Statistical analysis

Measurements taken before and after LOR and ROR were statistically compared from 120 s data windows preceding (PreLOR and PreROR) and following (LOR and ROR) the state transition points by two-tailed paired-sample *t*-tests (df = 17). Unless otherwise stated (e.g., uncorrected), p values with FDR correction ($\alpha < 0.05$) were reported. For subcorticocortical functional connectivity map in Fig. 5C, whole-brain voxel-wise paired sample t-tests (two-sided) between PreROR window and ROR window were performed at the group level. The resulting *z*-map was thresholded at the cluster level $\alpha < 0.05$. This was achieved using AFNI's upgraded function 3dttest ++ with the '-Clustsim' option that simulates noise volume assuming the spatial autocorrelation function is given by a mixed-model rather than a Gaussian-shaped function (Cox et al., 2017).

Results

Induction-emergence hysteresis in behavioral responsiveness

We found that the transition to unconsciousness (i.e., LOR by definition) occurred at a higher ESC than at the transition to regaining consciousness (i.e., ROR by definition) (Fig. 2A, 2C). This implied a delayed process in the recovery of behavioral responsiveness with respect to the same level of anesthetic dose at LOR (yellow shaded area in Fig. 2A). The test results were: PreLOR > PreROR: $t = 5.993$, $p < 0.0001$; PreLOR > ROR: $t = 8.553$, $p < 0.0001$; LOR > PreROR: $t = 6.411$, $p < 0.0001$; LOR > ROR: $t = 8.636$, $p < 0.0001$. By plotting the fraction of responsiveness (across subjects) vs. estimated propofol effect-site concentration (Fig. 2B), we observed a clear hysteresis loop, where the area between the curves of induction and emergence represents a resistance to change in the state of consciousness. These results are in line with prior studies suggesting a role for intrinsic neural dynamics impeding recovery (Friedman et al., 2010; Joiner et al., 2013).

Global changes of brain activity during state transitions

No statistically significant change of the globally-averaged autocorrelation index was found during the transition into LOR (PreLOR vs. LOR: $t = -2.099$, $p = 0.0510$), whereas the autocorrelation index showed a sharp drop toward baseline level upon ROR (PreROR > ROR: $t = 5.273$, $p < 0.0001$) (Fig. 2D–E). The globally-averaged strength centrality did not show any statistically significant change at the transition point for either transitioning into (PreLOR vs. LOR: $t = 1.892$, $p = 0.0756$) or out of LOR (PreROR vs. ROR: $t = 0.008$, $p = 0.9934$) (Fig. 2F–G). It is noteworthy that the time courses of ESC during induction and emergence were more or less symmetric (Fig. 2A), whereas the time courses of the temporal autocorrelation and strength centrality appeared to be asymmetric. This suggests that the pharmacokinetic effects cannot solely account for the difference in neural dynamics between induction and emergence.

Network changes of brain activity during state transitions

Next, we examined if there were specific changes of brain activity during the transition periods at the network level. First, we measured temporal autocorrelation, strength centrality, and within- and between-network functional connectivity in pre-defined networks (Huang et al., 2018a; Power et al., 2011). We found that the subcortical network was an exceptional case compared to all other networks during the transition periods. Specifically, it was the only network that did not show any statistically significant change in temporal autocorrelation at ROR (Fig. 3A). Furthermore, an abrupt increase of strength centrality (Fig. 3B), instead of within-network connectivity (Fig. 3C), was found only in the subcortical network at ROR. The increased strength centrality of the subcortical network can be characterized by an overall increase of between-network functional connectivity that related to the subcortical network (e.g., sensory/somatomotor – subcortical, cingulo/opercular task control – subcortical, auditory – subcortical, dorsal attention – subcortical) (Fig. 3D).

Regional distribution of brain activity changes during state transitions

To gain a more spatially detailed picture of changes, we extracted the autocorrelation index and strength centrality from 90 anatomical regions of interest based on the AAL atlas. Upon ROR the temporal autocorrelation abruptly decreased across the majority of cortical regions but not the subcortical regions (Fig. 4A). However, some of the subcortical regions, particularly the bilateral thalamus and pallidum, showed an abrupt boost of strength centrality at ROR (Fig. 4B). Together, these results indicate that regaining consciousness was associated with an abrupt restorative decrease of temporal autocorrelation in the cortex, and an abrupt boost of functional connectivity between subcortical and cortical regions.

Temporal trajectory of functional connectivity and temporal autocorrelation during state transitions

Brain activity from global to network to regional levels all pointed to distinct neural dynamics between cortical and subcortical regions during state transitions. To consolidate the above findings, we narrowed down the focus by presenting the results of cortex (taking it as a whole), thalamus and pallidum during the course of state transitions. Again, regaining

consciousness (ROR) was associated with an abrupt restoration of the cortical (not the thalamus or pallidum) temporal autocorrelation ($p = 0.00028$, FDR corrected), and an abrupt boost of thalamocortical ($p = 0.00041$, FDR corrected) and pallidocortical (p = 0.00038, FDR corrected) functional connectivity (Fig. 5A–B). When investigating the voxel level (the average fMRI time series across the entire cortex was used as a regressor), we found that the abrupt boost of subcorticocortical functional connectivity during restoration of consciousness included the brain stem and several basal ganglia and thalamic nuclei (Fig. 5C). Finally, to illustrate the temporal interdependence of these effects, the trajectory of group-averaged subcorticocortical functional connectivity (average of thalamocortical and pallidocortical functional connectivity) was plotted as a function of the group-averaged cortical signal's temporal autocorrelation. This plot clearly reveals an asymmetric trajectory of brain dynamics during LOR and ROR, illustrating how these state transitions occupy distinct zones of the trajectory space (Fig. 5D).

Control analyses

For methodological considerations regarding the issue of global signal regression (Murphy and Fox, 2017), we compared our results both with and without global signal regression (GSR). We found that the autocorrelation index (i.e., derived from local fMRI signals) was not substantially influenced by the presence or absence of GSR, albeit GSR enhanced the effects of interest to a greater or lesser degree (Fig. S1). On the contrary, applying the GSR procedure eliminated all the effects of interest in the functional connectivity measures, including strength centrality (Fig. S1) and its analogous measures (e.g., weighted degree centrality and binary degree centrality when applying an empirical threshold; Fig. S2), as well as within- and between-network functional connectivity (Fig. S3). Together, controlling shared signal across the whole brain (i.e., applying GSR procedure) may be beneficial for extracting the genuine local effects, whereas the preservation of the global component in the data (non-GSR) seemed to be important when studying distant functional connectivity related to different conscious states.

To evaluate whether the results of temporal autocorrelation could be affected by the selection of window length of the AUC, we varied the window length from 0.8 seconds (one TR) to 40 seconds (50 TRs). Supporting the main results in Fig. 5, the abrupt restoration of the cortical temporal autocorrelation upon ROR was invariant with respect to the selection of window length (Fig. S4).

Discussion

The goal of this investigation was to determine if time-dependent neural functional connectivity and the speed (timescale) of neural processing would reveal asymmetric neural dynamics during anesthetic state transitions in healthy human participants. Our data indeed revealed distinct neural dynamics during induction vs. emergence that differentiated the suppression and restoration of consciousness. We disentangled such asymmetric neural dynamics into three pairs of contrasting characteristics, i.e., gradual vs. abrupt, local neural timescale vs. distant connectivity, and subcortical vs. cortical. Specifically, we found that on the way to losing consciousness the local neural timescale of the entire brain gradually

increased, whereas distant functional connectivity gradually decreased. In contrast, regaining consciousness was associated with an abrupt restoration of cortical, but not subcortical, neural timescale and an abrupt boost of subcorticocortical functional connectivity. Because these findings cannot be explained by pharmacokinetic factors, they support the neural inertia hypothesis and may offer a specific neuronal account, i.e., asymmetric neural dynamics of subcorticocortical neural interactions.

Asymmetric neural dynamics during loss and recovery of consciousness

Increasing the propofol effect-site concentration *en route* to unconsciousness was accompanied by a gradual increase of the fMRI signal's temporal autocorrelation across the whole brain together with a gradual decrease of distant functional connectivity (e.g., strength centrality, within- and between-network connectivity). The increase of temporal autocorrelation presumably reflects an increase of local neuronal synchronization (Honey et al., 2012; Supp et al., 2011), reflecting the slowing of neural processing (Hasson et al., 2008; Lerner et al., 2011; Murray et al., 2014; Raut et al., 2020). In agreement with our prior observations (Huang et al., 2018a), we found that the increase of signal's temporal autocorrelation occurred prior to the decrease of distant functional connectivity (Fig. 2C–D). This supports our conclusion that propofol may synchronize local neuronal interactions and prolong the neural timescales, which in turn, disrupt information exchange among distant brain regions (Huang et al., 2018a). However, we did not find a significant change of those fMRI-derived quantities at the transition point of losing consciousness. This may be due to either that (1) the differential between adjacent data windows was too small to detect, or (2) losing consciousness itself is a gradual rather than abrupt process (Veselis, 2001). Of note, the increase of temporal autocorrelation followed by the decrease of global functional connectivity during anesthesia are highly reproducible results across our current and previous datasets analyzed by different protocols (see Fig. S4 comparable with (Huang et al., 2018a; Tanabe et al., 2020)).

Importantly, regaining consciousness was associated with an abrupt restoration (decrease to baseline level) of the cortical signal's temporal autocorrelation and an abrupt boost of subcorticocortical functional connectivity. These abrupt changes are of particular interest because they depict differential neural behaviors between thalamus and cortex. On one hand, the decrease of cortical temporal autocorrelation may indicate an increase in the speed of cortical neural processing. On the other hand, the boost of subcorticocortical functional connectivity may indicate a ramp-up of arousal (see below for more discussion). This is supported by previous findings showing a critical role of subcortical activation (e.g., brainstem and thalamus) during emergence from anesthesia in humans with fMRI (Nir et al., 2019) and PET (Långsjö et al., 2012; Scheinin et al., 2020). Taken together, we speculate that these processes may reflect a re-engagement of subcorticocortical and corticocortical loops necessary for the integration of bottom-up and top-down data streams (Aru et al., 2020; Bachmann and Hudetz, 2014; Mashour and Hudetz, 2018, 2017).

Admittedly, a firm causal relationship between the described events in thalamus and cortex is difficult to assert from our data because of the relatively limited temporal resolution of fMRI and the lack of direct neuronal evidence. However, combining our results with

additional evidence from electrophysiological studies (Flores et al., 2017; Patel et al., 2020), a shift to faster neural timescale and a jump-start of subcorticocortical neural interactions appear as plausible necessary steps in the mechanism of restoring consciousness. As previously found in a rodent study, emergence from propofol anesthesia was accompanied by an abrupt transition from slow delta-alpha to beta oscillations, which was distinct from the gradual transition during induction (Flores et al., 2017). A similar abrupt transition from slow delta and broadband alpha and beta oscillations to just beta oscillations occurred in the thalamus, again distinct from the gradual change during induction. A comparable abrupt shift of neuronal beta oscillations during emergence was seen in the primate neocortex (Patel et al., 2020).

Hysteresis and neural inertia

We found that LOR and ROR occurred at substantially different effect-site propofol concentrations. As a result, the propofol concentration - response relationship was not unique but followed distinct trajectories for the ascending vs. descending concentrations, forming a closed loop commonly known as hysteresis. Some of the early investigators attributed this hysteresis to a pharmacokinetic effect, i.e., a differential lag between plasma and effect site equilibration (McKay et al., 2006). However, more recent findings suggest that anesthetic hysteresis has a neurobiological explanation called neural inertia. Neural inertia refers to an intrinsic resistance of the brain to a change in state (Friedman et al., 2010; Joiner et al., 2013; Kelz et al., 2008; Kim et al., 2018; Patel et al., 2020; Steyn-Ross et al., 2004). This resistance results in a need for a greater concentration of the anesthetic to initiate the transition from PreLOR to LOR compared to that required to transition from PreROR to ROR.

The exact mechanism of neural inertia has not been conclusively determined. It may be mediated by specific neuronal populations that create an inertial barrier against state transitions in order to maintain or stabilize wakefulness or anesthesia (Friedman et al., 2010; Joiner et al., 2013). Specifically, it may be related to the neurons' bistability due to feedback, which commonly leads to hysteresis in biological systems (Chatterjee et al., 2008; Moreno-Bote et al., 2007; Steyn-Ross et al., 2004; Voss et al., 2012). Feedback between local neuronal populations or between functional brain regions may initiate state transitions and stabilization of the new state (Joiner et al., 2013). As an example, anesthetics may hijack the sleep-wake circuitry by exciting sleep-promoting and inhibiting wake-promoting neurons (McKinstry-Wu et al., 2019; Moore et al., 2012; Proekt and Hudson, 2018; Zhang et al., 2015). These neuronal populations mutually inhibit each other and thus exhibit self-reinforcing behavior (McKinstry-Wu et al., 2019). Once sleep-active neurons activate beyond a certain threshold, they shut down the wake-active neurons thereby decreasing their inhibitory effects and further strengthen mutual excitation amongst the sleep-active neurons (Proekt and Hudson, 2018; Saper et al., 2005). The converse happens during wakefulness. As another example, activation of the arousal system can make thalamocortical neurons switch from burst firing (characteristic of sleep and anesthesia) to tonic firing (characteristic of waking) (Fuentealba et al., 2005). This results in the recruitment of cortical neurons into a positive feedback loop that maintains the excitation of both sets of neurons, thus stabilizing the waking state (Joiner et al., 2013).

Mathematical models have also been developed to illustrate how anesthetic hysteresis (and neuronal inertia) may arise from neuronal bistability or multistability (Proekt and Hudson, 2018), and percolation phenomena (Su et al., 2020). Another mathematical model suggested that anesthetic hysteresis is a generic network feature, which is mediated by patterns of explosive synchronization, i.e., a discontinuous transition between incoherent and synchronized states of a network (Kim et al., 2018). Specifically, applying a large-scale brain network model, the authors demonstrated that the asymmetry of synchronization suppression could account for anesthetic hysteresis, where an adaptive feedback term (i.e., a recursive interaction process between brain regions) in the model plays an essential role in producing the asymmetric suppression. Nevertheless, the above brain network model only included cortical regions. Considering the role of subcorticocortical neural interactions in rebooting consciousness as shown by our data, we speculate that the subcortical regions may have unique contributions in generating brain-wide explosive synchronization. Future work that implements neuroanatomically informed subcorticocortical architecture into the brain network model may help testing this hypothesis.

To-date, clinical investigations of anesthetic hysteresis have yielded mixed results. Two forms of evidence have been considered: (1) anesthetic dose vs. behavioral responsiveness, and (2) anesthetic dose vs. brain-based measures. Regarding (1), anesthetic hysteresis was found during sevoflurane anesthesia (Kuizenga et al., 2018) but not during propofol anesthesia (Kuizenga et al., 2018; Warnaby et al., 2017), whereas three other studies supported anesthetic hysteresis during propofol anesthesia (Ferreira et al., 2020; Nir et al., 2019; Sepúlveda et al., 2019). Regarding (2), Warnaby and colleagues (Warnaby et al., 2017) found asymmetric EEG slow wave activity saturation during induction and emergence, which might be a signature of neural inertia. Furthermore, simultaneous EEG-fMRI showed that at the point of slow-wave activity saturation, stereotypical thalamocortical responses to nociceptive and auditory inputs were abolished (Mhuircheartaigh et al., 2013). Lewis and colleagues (Lewis et al., 2018) also identified an asymmetry during induction and emergence from propofol anesthesia, where the emerging brain could enter a state with a sleep-like sensory blockade (e.g., K-complexes) before regaining responsiveness to arousal stimuli. However, unlike slow-wave activity saturation or K-complexes, EEG/LFP spectral power (Breshears et al., 2010; Purdon et al., 2013) did not follow a clear pattern of hysteresis during propofol anesthesia. By visual inspection, the time course of EEG effective connectivity suggested some asymmetry between induction and emergence with propofol (Pullon et al., 2020), however this was not directly tested by the authors.

In our present work, both the behavioral and brain-based data support the existence of anesthetic hysteresis and favor the neural inertia concept. First, we observed a hysteresis loop between the anesthetic dose and behavioral responsiveness with the transition to unconsciousness occurring at a higher ESC than the transition to consciousness. Second, we observed hysteresis in the anesthetic dose vs. brain-based measures, i.e., in the subcorticocortical functional connectivity and cortical temporal autocorrelation. In addition, the abrupt boost of subcorticocortical functional connectivity following the hysteretic resistance to ROR may reflect the action of positive feedback and stabilization process.

Subcortical vs. cortical mechanisms

A long-standing debate in anesthesiology relates to the systemslevel mechanisms for anesthesia-induced unconsciousness. Two main hypotheses posit the disruption of either the corticocortical loops or thalamocortical loops (Alkire et al., 2008; Hudetz, 2012; Mashour, 2014; Mashour, 2006; Mashour and Hudetz, 2018, 2017; White and Alkire, 2003). Our results suggest that both hypotheses could be true but they likely correspond to different aspects of consciousness.

First, corticocortical functional connectivity, including both within- and between-network functional connectivity, changed in a graded fashion during state transitions. We speculate that the corticocortical changes during anesthesia may be more directly related to the suppression of awareness (the content of consciousness) rather than arousal (the level of consciousness). This is consistent with the theoretical framework of top-down and bottom-up mechanisms of general anesthetics mapping on to disruptions of content and level of consciousness, respectively (Mashour and Hudetz, 2017). Second, the abrupt boost of subcorticocortical connectivity upon emergence (ROR) involved the brain stem, basal ganglia and thalamic nuclei that participate in the brainstem-thalamocortical axis of arousal (Akeju et al., 2014; Fischer et al., 2016; Giacino et al., 2014; Gili et al., 2013; Halassa et al., 2014; Halassa and Kastner, 2017; Hindman et al., 2018; Mhuircheartaigh et al., 2010; Song et al., 2017). The basal ganglia are also involved in regulating thalamocortical signal transmission (Mhuircheartaigh et al., 2010; Schiff, 2010; Schiff et al., 2007) with the dorsal pallidum, in particular, regulating voluntary movement (Gillies et al., 2017). Thus, our data provide a plausible account for the involvement of subcorticocortical networks in the recovery of arousal and behavioral responsiveness.

Taken together, anesthetic-induced unconsciousness could be associated with the suppression of two functional architectures, the corticocortical loops and subcorticocortical arousal pathway. In the conscious brain, the dual functional architecture allows a dynamic integration of bottom-up and top-down data streams that converge arousal and awareness into unified conscious experience (Aru et al., 2020; Bachmann and Hudetz, 2014; Mashour and Hudetz, 2017). *En route* to unconsciousness, both functional systems may be gradually corrupted. Restoration of consciousness, on the other hand, may depend on the abrupt neural activation of arousal pathways, accompanied by an abrupt restoration of neural timescales in the cortex.

Clinical implications

Recent studies indicated that there might be shared neural pathways between pharmacologic and pathologic states of unconsciousness (coma or persistent vegetative states), such that the former may inform the clinical diagnosis of the latter (Campbell et al., 2020; Huang et al., 2020; Tanabe et al., 2020). It has also been suggested that the feedback and bistability involved in neural inertia may be impaired in pathologic states of unconsciousness, and the neural inertial barrier separating waking from unconscious states may be widened beyond the range of reversibility normally associated with physiological processes (Joiner et al., 2013). Therefore, establishing a pharmacologic “coma” model in humans and targeting the brainstem-thalamocortical arousal pathway, as suggested by our data, may potentially

benefit the development of therapeutic interventions in patients with disorders of consciousness, such as through thalamic stimulation in brain injured patients (Schiff et al., 2007). In this respect, there is evidence from animal studies that microinjection of nicotine (Alkire et al., 2007) or antibodies blocking a voltage-gated potassium channel (Alkire et al., 2009) into the central medial thalamus of rats or central thalamic electrical stimulation in primates (Redinbaugh et al., 2020) can awaken the animals in spite of the continued administration of an anesthetic. Activation of other subcortical arousal pathways that project in part to the thalamus may also play a role. For example, muscarinic cholinergic activation of the basal forebrain (Hudetz et al., 2003), electrical or optogenetic stimulation of the ventral tegmental area (Solt et al., 2014; Taylor et al., 2016) and parabrachial area (Muindi et al., 2016; Wang et al., 2019) facilitate “reanimation” from anesthesia. Pharmacological disinhibition of the medullary reticular activating system triggers emergence from both anesthesia and hypoglycemic coma (Gao et al., 2019). Besides these subcortical interventions, direct pharmacological stimulation of prefrontal cortex has been shown to reverse general anesthesia and restore full wakefulness in rats (Pal et al., 2018). This demonstrated a crucial role of prefrontal cortex positioned along the mesocircuit involving the thalamus, globus pallidus, striatum, and basal forebrain (Knotts et al., 2018).

Neural inertia appears to provide a natural resistance to rapid and potentially catastrophic transitions between states such as wake-to-sleep transitions observed in patients with narcolepsy (Lu et al., 2006). Nevertheless, there may be circumstances with a need to mitigate the effect of neural inertia, “inducing emergence” to achieve control over the process that parallels that of inducing anesthesia (Tarnal et al., 2016). Hence, identifying the neural mechanisms that mediate the resistance to state transitions and recovery from general anesthesia may ultimately lead to novel therapies via selectively stabilizing the anesthetized state and avoiding anesthetic overdose, or selectively destabilizing the state of anesthesia at the end of surgery to facilitate recovery.

Limitations

Our study has a number of limitations. First, consciousness was operationally indexed by behavioral responsiveness. The nomenclature of LOR and ROR followed the experimental definition. Although we surmise that intact responsiveness indicates consciousness, this is not certain due to the possibility of covert consciousness (Monti et al., 2010; Owen et al., 2006). Likewise, unresponsiveness does not strictly necessitate unconsciousness (Sanders et al., 2012), although this is often inferred. Second, because the effect-site concentration of propofol cannot be directly measured in healthy volunteers, it was estimated from a pharmacokinetic model (Marsh et al., 1991), which may not accurately reflect the exact drug concentration in the brain. This makes it difficult to provide irrefutable evidence for or against the existence of hysteresis in humans. In prior considerations, by simply adjusting pharmacokinetic–pharmacodynamic (PK-PD) parameters (Baars et al., 2006; Kuizenga et al., 2001), one could either conclude that hysteresis either does or does not exist based upon identical behavioral observations (Proekt and Kelz, 2020). Nevertheless, given the phylogenetic conservation of neural inertia as found in other species ranging from invertebrates to vertebrates (Friedman et al., 2010; Joiner et al., 2013), the preponderance of evidence suggests that anesthetic hysteresis indeed exists. Third, neural changes during the

course of losing versus regaining consciousness can be best examined when the depth of anesthesia is varied slowly or incrementally, as implemented in our study, but this protocol is not generally used in clinical practice. This approach has, nevertheless, exclusive power to reveal the potential difference in neural dynamics between anesthetic induction and emergence. Fourth, a previous investigation found a decrease of the Hurst exponent – another measure of temporal autocorrelation – in monkeys anesthetized with propofol (Barttfeld et al., 2015). Compared to this, we found that propofol sedation at low effect-site concentration (ESC = ~2.4 μg/ml) globally increased temporal autocorrelation and our former study, analyzing an independent dataset at ESC = ~1.9 μg/ml, found the same effect (Huang et al., 2018a). However, a deeper level of propofol anesthesia (ESC = 4.0 μg/ml) leads to a global decline of temporal autocorrelation, e.g., Fig. 7 in (Huang et al., 2018a). Since Barttfeld et al. applied high ESC at 3.7–6.5 μg/ml, their finding of diminished Hurst exponent is consistent with our former results and is not in conflict with our current finding obtained at a much lower ESC. Nevertheless, the neural mechanism of a biphasic phenomenon of temporal autocorrelation during the course of sedation and anesthesia, i.e., increases at low ESC and decreases at high ESC, remains largely unknown and therefore warrants further examination. Fifth, there seemed to be corticocortical network changes preceding the subcorticocortical changes. For example, in Fig. 5B, a trend of increase in corticocortical functional connectivity occurred a few minutes prior to the abrupt change of subcorticocortical functional connectivity upon ROR. Although this phenomenon is interesting, we were not able to ascertain if there was a causal relationship between the early corticocortical changes and the late subcorticocortical changes. One possibility is that the former drove the latter. Another possibility is that they were parallel processes, where corticocortical changes reflected recovery associated with the decrease of propofol concentration, whereas the subcorticocortical changes were associated with neural inertia (a time delay by definition) that determines behavioral responsiveness. Lastly, different anesthetic agents may alter neural dynamics in different ways. Whether our results can be generalized to anesthetics of different pharmacological class including halogenated ethers or non-GABAergic drugs such as ketamine remains to be determined. However, prior studies from our research group using computational modeling and empirical neurophysiologic data in humans exposed to sevoflurane and ketamine support asymmetric network dynamics as a source of observed hysteresis (Kim et al., 2018).

Conclusions

We conclude that losing and regaining consciousness follows asymmetric neural dynamics. A rapid increase in the speed of cortical neural processing with a jump-start of subcorticocortical functional connectivity may account for rebooting consciousness after anesthesia. Our findings support the neural inertia hypothesis and offer a specific neuronal account.

Supplementary Material

Refer to Web version on PubMed Central for supplementary material.

Acknowledgments

This study was supported by a grant from the National Institute of General Medical Sciences of the NIH under award R01-GM103894 (to A.G.H.). The content is solely the responsibility of the authors and does not necessarily represent the official views of the NIH.

Data availability

Original data that support the findings of this study are available from the corresponding authors (Z.H. and A.G.H.) upon reasonable request.

References

Adapa RM, Davis MH, Stamatakis EA, Absalom AR, Menon DK, 2014. Neural correlates of successful semantic processing during propofol sedation. Hum. Brain Mapp 35, 2935–2949. doi: 10.1002/hbm.22375. [PubMed: 24142410]

Akeju O, Loggia ML, Catana C, Pavone KJ, Vazquez R, Rhee J, Contreras Ramirez V, Chonde DB, Izquierdo-Garcia D, Arabasz G, Hsu S, Habeeb K, Hooker JM, Napadow V, Brown EN, Purdon PL, Ramirez VC, Chonde DB, Izquierdo-Garcia D, Arabasz G, Hsu S, Habeeb K, Hooker JM, Napadow V, Brown EN, Purdon PL, 2014. Disruption of thalamic functional connectivity is a neural correlate of dexmedetomidine-induced unconsciousness. In: Elife, 3, p. e04499. doi: 10.7554/eLife.04499. [PubMed: 25432022]

Alkire MT, Asher CD, Franciscus AM, Hahn EL, 2009. Thalamic microinfusion of antibody to a voltage-gated potassium channel restores consciousness during anesthesia. Anesthesiology 110, 766–773. doi: 10.1097/ALN.0b013e31819c461c. [PubMed: 19322942]

Alkire MT, Hudetz AG, Tononi G, 2008. Consciousness and anesthesia. Science 322, 876–880. doi: 10.1126/science.1149213. [PubMed: 18988836]

Alkire MT, McReynolds JR, Hahn EL, Trivedi AN, 2007. Thalamic microinjection of nicotine reverses sevoflurane-induced loss of righting reflex in the rat. Anesthesiology 107, 264–272. doi: 10.1097/01.anes.0000270741.33766.24. [PubMed: 17667571]

Aru J, Suzuki M, Larkum ME, 2020. Cellular mechanisms of conscious processing. Trends Cogn. Sci doi: 10.1016/j.tics.2020.07.006.

Baars JH, Dangel C, Herold KF, Hadzidiakos DA, Rehberg B, 2006. Suppression of the human spinal H-reflex by propofol: a quantitative analysis. Acta Anaesthesiol. Scand 50, 193–200. doi: 10.1111/j.1399-6576.2006.00923.x. [PubMed: 16430541]

Bachmann T, Hudetz AG, 2014. It is time to combine the two main traditions in the research on the neural correlates of consciousness: C = LxD. Front. Psychol 5, 1–13. doi: 10.3389/fpsyg.2014.00940. [PubMed: 24474945]

Barttfeld P, Uhrig L, Sitt JD, Sigman M, Jarraya B, Dehaene S, 2015. Signature of consciousness in the dynamics of resting-state brain activity. Proc. Natl. Acad. Sci. U. S. A 112, E5219–E5220. doi: 10.1073/pnas.1515029112. [PubMed: 26324930]

Bonhomme V, Vanhaudenhuyse A, Demertzi A, Bruno MA, Jaquet O, Bahri MA, Plenevaux A, Boly M, Boveroux P, Soddu A, Brichant JF, Maquet P, Laureys S, 2016. Resting-state network-specific breakdown of functional connectivity during ketamine alteration of consciousness in volunteers. Anesthesiology 125, 873–888. doi: 10.1097/ALN.0000000000001275. [PubMed: 27496657]

Boveroux P, Vanhaudenhuyse A, Bruno MAA, Noirhomme Q, Lauwick S, Luxen A, Degueldre C, Plenevaux A, Schnakers C, Phillips C, Brichant JFF, Bonhomme V, Maquet P, Greicius MD, Laureys S, Boly M, 2010. Breakdown of within- and between-network resting state functional magnetic resonance imaging connectivity during propofol-induced loss of consciousness. Anesthesiology 113, 1038–1053. doi: 10.1097/ALN.0b013e3181f697f5. [PubMed: 20885292]

Breshears JD, Roland JL, Sharma M, Gaona CM, Freudenburg ZV, Tempelhoff R, Avidan MS, Leuthardt EC, 2010. Stable and dynamic cortical electrophysiology of induction and emergence with propofol anesthesia. Proc. Natl. Acad. Sci. USA 107, 21170–21175. doi: 10.1073/pnas.1011949107. [PubMed: 21078987]

Campbell JM, Huang Z, Zhang J, Wu X, Qin P, Northoff G, Mashour GA, Hudetz AG, 2020. Pharmacologically informed machine learning approach for identifying pathological states of unconsciousness via resting-state fMRI. Neuroimage 206, 116316. doi: 10.1016/j.neuroimage.2019.116316. [PubMed: 31672663]

Chatterjee A, Kaznessis YN, Hu WS, 2008. Tweaking biological switches through a better understanding of bistability behavior. Curr. Opin. Biotechnol 19, 475–481. doi: 10.1016/j.copbio.2008.08.010. [PubMed: 18804166]

Cox RW, Chen G, Glen DR, Reynolds RC, Taylor PA, 2017. FMRI clustering in AFNI: false-positive rates redux. Brain Connect 7, 152–171. doi: 10.1089/brain.2016.0475. [PubMed: 28398812]

Davis MH, Coleman MR, Absalom AR, Rodd JM, Johnsrude IS, Matta BF, Owen AM, Menon DK, 2007. Dissociating speech perception and comprehension at reduced levels of awareness. Proc. Natl. Acad. Sci. USA 104, 16032–16037. doi: 10.1073/pnas.0701309104. [PubMed: 17938125]

Demertzi A, Tagliazucchi E, Dehaene S, Deco G, Barttfeld P, Raimondo F, Martial C, Fernández-Espejo D, Rohaut B, Voss HU, Schiff ND, Owen AM, Laureys S, Naccache L, Sitt JD, 2019. Human consciousness is supported by dynamic complex patterns of brain signal coordination. Sci. Adv 5, eaat7603. doi: 10.1126/sciadv.aat7603. [PubMed: 30775433]

Dueck MH, Petzke F, Gerbershagen HJ, Paul M, Heßelmann V, Girnus R, Krug B, Sorger B, Goebel R, Lehrke R, Sturm V, Boerner U, 2005. Propofol attenuates responses of the auditory cortex to acoustic stimulation in a dose-dependent manner: a FMRI study. Acta Anaesthesiol. Scand 49, 784–791. doi: 10.1111/j.1399-6576.2005.00703.x. [PubMed: 15954960]

Ferreira AL, Correia R, Vide S, Ferreira AD, Kelz MB, Mendes JG, Nunes CS, Amorim P, 2020. Patterns of hysteresis between induction and emergence of neuroanesthesia are present in spinal and intracranial surgeries. J. Neurosurg. Anesthesiol 32, 82–89. doi: 10.1097/ANA.0000000000000559. [PubMed: 30371631]

Fischer DB, Boes AD, Demertzi A, Evrard HC, Laureys S, Edlow BL, Liu H, Saper CB, Pascual-Leone A, Fox MD, Geerling JC, 2016. A human brain network derived from coma-causing brainstem lesions. Neurology 87, 2427–2434. doi: 10.1212/WNL.0000000000003404. [PubMed: 27815400]

Fiset P, Daloze T, Plourde G, Meuret P, Bonhomme V, Hajj-ali N, Backman SB, Evans AC, 1999. Brain mechanisms of propofol-induced loss of consciousness in humans: a positron emission tomographic study. J. Neurosci 19, 5506–5513. doi: 10.1523/JNEUROSCI.19-13-05506.1999. [PubMed: 10377359]

Flores FJ, Hartnack KE, Fath AB, Kim SE, Wilson MA, Brown EN, Purdon PL, 2017. Thalamocortical synchronization during induction and emergence from propofol-induced unconsciousness. Proc. Natl. Acad. Sci. USA 114, E6660–E6668. doi: 10.1073/pnas.1700148114. [PubMed: 28743752]

Friedman EB, Sun Y, Moore JT, Hung HT, Meng QC, Perera P, Joiner WJ, Thomas SA, Eckenhoff RG, Sehgal A, Kelz MB, 2010. A conserved behavioral state barrier impedes transitions between anesthetic-induced unconsciousness and wakefulness: evidence for neural inertia. PLoS One 5, e11903. doi: 10.1371/journal.pone.0011903. [PubMed: 20689589]

Fuentealba P, Timofeev I, Bazhenov M, Sejnowski TJ, Steriade M, 2005. Membrane bistability in thalamic reticular neurons during spindle oscillations. J. Neurophysiol 93, 294–304. doi: 10.1152/jn.00552.2004. [PubMed: 15331618]

Gao S, Proekt A, Renier N, Calderon DP, Pfaff DW, 2019. Activating an anterior nucleus gigantocellularis subpopulation triggers emergence from pharmacologically-induced coma in rodents. Nat. Commun 10, 2897. doi: 10.1038/s41467-019-10797-7. [PubMed: 31263107]

Giacino JT, Fins JJ, Laureys S, Schiff ND, 2014. Disorders of consciousness after acquired brain injury: the state of the science. Nat. Rev. Neurol 10, 99–114. doi: 10.1038/nrneurol.2013.279. [PubMed: 24468878]

Gili T, Saxena N, Diukova A, Murphy K, Hall JE, Wise RG, 2013. The thalamus and brainstem act as key hubs in alterations of human brain network connectivity induced by mild propofol sedation. J. Neurosci 33, 4024–4031. doi: 10.1523/JNEUROSCI.3480-12.2013. [PubMed: 23447611]

Gillies MJ, Hyam JA, Weiss AR, Antoniades CA, Bogacz R, Fitzgerald JJ, Aziz TZ, Whittington MA, Green AL, 2017. The cognitive role of the globus pallidus interna; Insights from disease states. Exp. Brain Res 235, 1455–1465. doi: 10.1007/s00221-017-4905-8. [PubMed: 28246967]

Gross WL, Lauer KK, Liu X, Roberts CJ, Liu S, Gollapudy S, Binder JR, Li SJ, Hudetz AG, 2019. Propofol sedation alters perceptual and cognitive functions in healthy volunteers as revealed by functional magnetic resonance imaging. Anesthesiology 131, 254–265. doi: 10.1097/ALN.0000000000002669. [PubMed: 31314747]

Halassa MM, Chen Z, Wimmer RD, Brunetti PM, Zhao S, Zikopoulos B, Wang F, Brown EN, Wilson MA, 2014. State-dependent architecture of thalamic reticular subnetworks. Cell 158, 808–821. doi: 10.1016/j.cell.2014.06.025. [PubMed: 25126786]

Halassa MM, Kastner S, 2017. Thalamic functions in distributed cognitive control. Nat. Neurosci 20, 1669–1679. doi: 10.1038/s41593-017-0020-1. [PubMed: 29184210]

Hasson U, Yang E, Vallines I, Heeger DJ, Rubin N, 2008. A hierarchy of temporal receptive windows in human cortex. J. Neurosci 28, 2539–2550. doi: 10.1523/JNEUROSCI.5487-07.2008. [PubMed: 18322098]

Hindman J, Bowren MD, Bruss J, Wright B, Geerling JC, Boes AD, 2018. Thalamic strokes that severely impair arousal extend into the brainstem. Ann. Neurol 84, 926–930. doi: 10.1002/ana.25377. [PubMed: 30421457]

Hindriks R, Adhikari MH, Murayama Y, Ganzetti M, Mantini D, Logothetis NK, Deco G, 2016. Can sliding-window correlations reveal dynamic functional connectivity in resting-state fMRI? Neuroimage 127, 242–256. doi: 10.1016/j.neuroimage.2015.11.055. [PubMed: 26631813]

Honey CJ, Thesen T, Donner TH, Silbert LJ, Carlson CE, Devinsky O, Doyle WK, Rubin N, Heeger DJ, Hasson U, 2012. Slow cortical dynamics and the accumulation of information over long timescales. Neuron 76, 423–434. doi: 10.1016/j.neuron.2012.08.011. [PubMed: 23083743]

Huang Z, Liu X, Mashour GA, Hudetz AG, 2018a. Timescales of intrinsic BOLD signal dynamics and functional connectivity in pharmacologic and neuropathologic states of unconsciousness. J. Neurosci 38, 2304–2317. doi: 10.1523/JNEUROSCI.2545-17.2018. [PubMed: 29386261]

Huang Z, Vlisides PE, Tarnal VC, Janke EL, Keefe KM, Collins MM, McKinney AM, Picton P, Harris RE, Mashour GA, Hudetz AG, 2018b. Brain imaging reveals covert consciousness during behavioral unresponsiveness induced by propofol. Sci. Rep 8, 13195. doi: 10.1038/s41598-018-31436-z. [PubMed: 30181567]

Huang Z, Zhang J, Wu J, Mashour GA, Hudetz AG, 2020. Temporal circuit of macroscale dynamic brain activity supports human consciousness. Sci. Adv 6, eaaz0087. doi: 10.1126/sciadv.aaz0087. [PubMed: 32195349]

Huang Z, Zhang JJ, Wu J, Qin P, Wu X, Wang Z, Dai R, Li Y, Liang W, Mao Y, Yang Z, Zhang JJ, Wolff A, Northoff G, 2016. Decoupled temporal variability and signal synchronization of spontaneous brain activity in loss of consciousness: an fMRI study in anesthesia. Neuroimage 124, 693–703. doi: 10.1016/j.neuroimage.2015.08.062. [PubMed: 26343319]

Hudetz AG, 2012. General anesthesia and human brain connectivity. Brain Connect 2, 291–302. doi: 10.1089/brain.2012.0107. [PubMed: 23153273]

Hudetz AG, Pillay S, Wang S, Lee H, 2020. Desflurane anesthesia alters cortical layer– specific hierarchical interactions in rat cerebral cortex. Anesthesiology 132, 1080–1090. doi: 10.1097/aln.0000000000003179. [PubMed: 32101967]

Hudetz AG, Wood JD, Kampine JP, 2003. Cholinergic reversal of isoflurane anesthesia in rats as measured by cross-approximate entropy of the electroencephalogram. Anesthesiology 99, 1125–1131. doi: 10.1097/00000542-200311000-00019. [PubMed: 14576549]

Hutchison RM, Womelsdorf T, Allen EA, Bandettini PA, Calhoun VD, Corbetta M, Della Penna S, Duyn JH, Glover GH, Gonzalez-Castillo J, Handwerker DA, Keilholz S, Kiviniemi V, Leopold DA, de Pasquale F, Sporns O, Walter M, Chang C, 2013. Dynamic functional connectivity: Promise, issues, and interpretations. Neuroimage 80, 360–378. doi: 10.1016/j.neuroimage.2013.05.079. [PubMed: 23707587]

Joiner WJ, Friedman EB, Hung HT, Koh K, Sowcik M, Sehgal A, Kelz MB, 2013. Genetic and anatomical basis of the barrier separating wakefulness and anesthetic-induced unresponsiveness. PLoS Genet 9, e1003605. doi: 10.1371/journal.pgen.1003605. [PubMed: 24039590]

Kelz MB, Sun Y, Chen J, Qing CM, Moore JT, Veasey SC, Dixon S, Thornton M, Funato H, Yanagisawa M, 2008. An essential role for orexins in emergence from general anesthesia. Proc. Natl. Acad. Sci. USA 105, 1309–1314. doi: 10.1073/pnas.0707146105. [PubMed: 18195361]

Kim H, Moon JY, Mashour GA, Lee UC, 2018. Mechanisms of hysteresis in human brain networks during transitions of consciousness and unconsciousness: Theoretical principles and empirical evidence. PLoS Comput. Biol 14, e1006424. doi: 10.1371/journal.pcbi.1006424. [PubMed: 30161118]

Knotts JD, Odegaard B, Lau H, 2018. Neuroscience: the key to consciousness may not be under the streetlight. Curr. Biol 28, R749–R752. doi: 10.1016/j.cub.2018.05.033. [PubMed: 29990459]

Kondo Y, Hirose N, Maeda T, Suzuki T, Yoshino A, Katayama Y, 2016. Changes in cerebral blood flow and oxygenation during induction of general anesthesia with sevoflurane versus propofol. Adv. Exp. Med. Biol 876, 479–484. doi: 10.1007/978-1-4939-3023-4. [PubMed: 26782248]

Kuizenga K, Proost JH, Wierda JM, Kalkman CJ, 2001. Predictability of processed electroencephalography effects on the basis of pharmacokinetic-pharmacodynamic modeling during repeated propofol infusions in patients with extradural analgesia. Anesthesiology 95, 607–615. doi: 10.1097/00000542-200109000-00011. [PubMed: 11575531]

Kuizenga MH, Colin PJ, Reyntjens KMEM, Touw DJ, Nalbat H, Knotnerus FH, Vereecke HEM, Struys MMRF, 2018. Test of neural inertia in humans during general anaesthesia. Br. J. Anaesth 120, 525–536. doi: 10.1016/j.bja.2017.11.072. [PubMed: 29452809]

Långsjö JW, Alkire MT, Kaskinoro K, Hayama H, Maksimow A, Kaisti KK, Aalto S, Aantaa R, Jääskeläinen SK, Revonsuo A, Scheinin H, 2012. Returning from oblivion: Imaging the neural core of consciousness. J. Neurosci 32, 4935–4943. doi: 10.1523/JNEUROSCI.4962-11.2012. [PubMed: 22492049]

Laumann TO, Snyder AZ, Mitra A, Gordon EM, Gratton C, Adeyemo B, Gilmore AW, Nelson SM, Berg JJ, Greene DJ, McCarthy JE, Tagliazucchi E, Laufs H, Schlaggar BL, Dosenbach NUF, Petersen SE, 2017. On the stability of BOLD fMRI correlations. Cereb. Cortex 27, 4719–4732. doi: 10.1093/cercor/bhw265. [PubMed: 27591147]

Lerner Y, Honey CJ, Silbert LJ, Hasson U, 2011. Topographic mapping of a hierarchy of temporal receptive windows using a narrated story. J. Neurosci 31, 2906–2915. doi: 10.1523/JNEUROSCI.3684-10.2011. [PubMed: 21414912]

Lewis LD, Piantoni G, Peterfreund RA, Eskandar EN, Harrell PG, Akeju O, Aglio LS, Cash SS, Brown EN, Mukamel EA, Purdon PL, 2018. A transient cortical state with sleep-like sensory responses precedes emergence from general anesthesia in humans. Elife 7, e33250. doi: 10.7554/eLife.33250. [PubMed: 30095069]

Lichtner G, Auksztulewicz R, Kirilina E, Velten H, Mavrodis D, Scheel M, Blankenburg F, von Dincklage F, 2018. Effects of propofol anesthesia on the processing of noxious stimuli in the spinal cord and the brain. Neuroimage 172, 642–653. doi: 10.1016/j.neuroimage.2018.02.003. [PubMed: 29421324]

Liu X, Lauer KK, Ward BD, Rao SM, Li SJ, Hudetz AG, 2012. Propofol disrupts functional interactions between sensory and high-order processing of auditory verbal memory. Hum. Brain Mapp 33, 2487–2498. doi: 10.1002/hbm.21385. [PubMed: 21932265]

Lu J, Sherman D, Devor M, Saper CB, 2006. A putative flip-flop switch for control of REM sleep. Nature 441, 589–594. doi: 10.1038/nature04767. [PubMed: 16688184]

Marsh B, White M, Morton N, Kenny GNC, 1991. Pharmacokinetic model driven infusion of propofol in children. Br. J. Anaesth 67, 41–48. doi: 10.1093/bja/67.1.41. [PubMed: 1859758]

Mashour GA, 2014. Top-down mechanisms of anesthetic-induced unconsciousness. Front. Syst. Neurosci 8, 115. doi: 10.3389/fnsys.2014.00115. [PubMed: 25002838]

Mashour GA, 2006. Integrating the science of consciousness and anesthesia. Anesth. Analg 103, 975–982. doi: 10.1213/01.ane.0000232442.69757.4a. [PubMed: 17000815]

Mashour GA, Hudetz AG, 2018. Neural correlates of unconsciousness in large-scale brain networks. Trends Neurosci 41, 150–160. doi: 10.1016/j.tins.2018.01.003. [PubMed: 29409683]

Mashour GA, Hudetz AG, 2017. Bottom-up and top-down mechanisms of general anesthetics modulate different dimensions of consciousness. Front. Neural Circuits 11, 44. doi: 10.3389/fncir.2017.00044. [PubMed: 28676745]

McKay IDH, Voss LJ, Sleigh JW, Barnard JP, Johannsen EK, 2006. Pharmacokinetic-pharmacodynamic modeling the hypnotic effect of sevoflurane using the spectral entropy of the

electroencephalogram. Anesth. Analg 102, 91–97. doi: 10.1213/01.ane.0000184825.65124.24. [PubMed: 16368811]

McKinstry-Wu AR, Wasilczuk AZ, Harrison BA, Bedell VM, Sridharan MJ, Breig JJ, Pack M, Kelz MB, Proekt A, 2019. Analysis of stochastic fluctuations in responsiveness is a critical step toward personalized anesthesia. Elife 8, e50143. doi: 10.7554/eLife.50143. [PubMed: 31793434]

Mhuircheartaigh RN, Rosenorn-Lanng D, Wise R, Jbabdi S, Rogers R, Tracey I, 2010. Cortical and subcortical connectivity changes during decreasing levels of consciousness in humans: a functional magnetic resonance imaging study using propofol. J. Neurosci 30, 9095–9102. doi: 10.1523/JNEUROSCI.5516-09.2010. [PubMed: 20610743]

Mhuircheartaigh RN, Warnaby C, Rogers R, Jbabdi S, Tracey I, 2013. Slow-wave activity saturation and thalamocortical isolation during propofol anesthesia in humans. Sci. Transl. Med 5, 208ra148. doi: 10.1126/scitranslmed.3006007.

Monti MM, Vanhaudenhuyse A, Coleman MR, Boly M, Pickard JD, Tshibanda L, Owen AM, Laureys S, 2010. Willful modulation of brain activity in disorders of consciousness. N. Engl. J. Med 362, 579–589. doi: 10.1056/NEJMoa0905370. [PubMed: 20130250]

Moore JT, Chen J, Han B, Meng QC, Veasey SC, Beck SG, Kelz MB, 2012. Direct activation of sleep-promoting VLPO neurons by volatile anesthetics contributes to anesthetic hypnosis. Curr. Biol 22, 2008–2016. doi: 10.1016/j.cub.2012.08.042. [PubMed: 23103189]

Moreno-Bote R, Rinzel J, Rubin N, 2007. Noise-induced alternations in an attractor network model of perceptual bistability. J. Neurophysiol 98, 1125–1139. doi: 10.1152/jn.00116.2007. [PubMed: 17615138]

Muindi F, Kenny JD, Taylor NE, Solt K, Wilson MA, Brown EN, Van Dort CJ, 2016. Electrical stimulation of the parabrachial nucleus induces reanimation from isoflurane general anesthesia. Behav. Brain Res 306, 20–25. doi: 10.1016/j.bbr.2016.03.021. [PubMed: 26971629]

Murphy K, Fox MD, 2017. Towards a consensus regarding global signal regression for resting state functional connectivity MRI. Neuroimage 154, 169–173. doi: 10.1016/j.neuroimage.2016.11.052. [PubMed: 27888059]

Murray JD, Bernacchia A, Freedman DJ, Romo R, Wallis JD, Cai X, Padoa-Schioppa C, Pasternak T, Seo H, Lee D, Wang XJ, 2014. A hierarchy of intrinsic timescales across primate cortex. Nat. Neurosci 17, 1661–1663. doi: 10.1038/nn.3862. [PubMed: 25383900]

Nir T, Or-Borichev A, Izraitel E, Hendler T, Lerner Y, Matot I, 2019. Transient subcortical functional connectivity upon emergence from propofol sedation in human male volunteers: evidence for active emergence. Br. J. Anaesth 123, 298–308. doi: 10.1016/j.bja.2019.05.038. [PubMed: 31277837]

Owen AM, Coleman MR, Boly M, Davis MH, Laureys S, Pickard JD, Pickard JD, 2006. Detecting awareness in the vegetative state. Science 313, 1402. doi: 10.1126/science.1130197. [PubMed: 16959998]

Pal D, Dean JG, Liu T, Li D, Watson CJ, Hudetz AG, Mashour GA, 2018. Differential role of prefrontal and parietal cortices in controlling level of consciousness. Curr. Biol 28. doi: 10.1016/j.cub.2018.05.025,2145-2152.e5.

Patel SR, Ballesteros JJ, Ahmed OJ, Huang P, Briscoe J, Eskandar EN, Ishizawa Y, 2020. Dynamics of recovery from anaesthesia-induced unconsciousness across primate neocortex. Brain 143, 833–843. doi: 10.1093/brain/awaa017. [PubMed: 32049333]

Power JD, Cohen AL, Nelson SM, Wig GS, Barnes KA, Church JA, Vogel AC, Laumann TO, Miezin FM, Schlaggar BL, Petersen SE, 2011. Functional network organization of the human brain. Neuron 72, 665–678. doi: 10.1016/j.neuron.2011.09.006. [PubMed: 22099467]

Proekt A, Hudson AE, 2018. A stochastic basis for neural inertia in emergence from general anaesthesia. Br. J. Anaesth 121, 86–94. doi: 10.1016/j.bja.2018.02.035. [PubMed: 29935600]

Proekt A, Kelz MB, 2018. Schrödinger's cat: anaesthetised and not! Br. J. Anaesth 120, 424–428. doi: 10.1016/j.bja.2017.11.068. [PubMed: 29452795]

Proekt A, Kelz MB, 2020. Explaining anaesthetic hysteresis with effect-site equilibration. Br. J. Anaesth 126, 265–278. doi: 10.1016/j.bja.2020.09.022. [PubMed: 33081972]

Pullon RM, Yan L, Sleigh JW, Warnaby CE, 2020. Granger causality of the electroencephalogram reveals abrupt global loss of cortical information flow during propofol-induced loss of

responsiveness. Anesthesiology 133, 774–786. doi: 10.1097/ALN.0000000000003398. [PubMed: 32930729]

Purdon PL, Pierce ET, Mukamel EA, Prerau MJ, Walsh JL, Wong KFK, Salazar-Gomez AF, Harrell PG, Sampson AL, Cimenser A, Ching S, Kopell NJ, Tavares-Stoeckel C, Habeeb K, Merhar R, Brown EN, Pascual-Leone A, 2013. Electroencephalogram signatures of loss and recovery of consciousness from propofol. Proc. Natl. Acad. Sci. USA 110, E1142–E1151. doi: 10.1073/pnas.1221180110. [PubMed: 23487781]

Raut RV, Snyder AZ, Raichle ME, 2020. Hierarchical dynamics as a macroscopic organizing principle of the human brain. Proc. Natl. Acad. Sci. USA 117, 20890–20897. doi: 10.1073/pnas.2003383117. [PubMed: 32817467]

Redinbaugh MJ, Phillips JM, Kambi NA, Mohanta S, Andryk S, Dooley GL, Afrasiabi M, Raz A, Saalmann YB, 2020. Thalamus modulates consciousness via layer-specific control of cortex. Neuron 106. doi: 10.1016/j.neuron.2020.01.005,66-75.e12.

Sanders RD, Tononi G, Laureys S, Sleigh JW, 2012. Unresponsiveness ≠ unconsciousness. Anesthesiology 116, 946–959. doi: 10.1097/ALN.0b013e318249d0a7. [PubMed: 22314293]

Saper CB, Scammell TE, Lu J, 2005. Hypothalamic regulation of sleep and circadian rhythms. Nature 437, 1257–1263. doi: 10.1038/nature04284. [PubMed: 16251950]

Scheinin A, Kantonen O, Alkire M, Långsjö J, Kallionpää RE, Kaisti K, Radek L, Johansson J, Sandman N, Nyman M, Scheinin M, Vahlberg T, Revonsuo A, Valli K, Scheinin H, 2020. Foundations of human consciousness: Imaging the twilight zone. J. Neurosci 41, 1769–1778. doi: 10.1523/jneurosci.0775-20.2020. [PubMed: 33372062]

Schiff ND, 2010. Recovery of consciousness after brain injury: a mesocircuit hypothesis. Trends Neurosci 33, 1–9. doi: 10.1016/j.tins.2009.11.002. [PubMed: 19954851]

Schiff ND, Giacino JT, Kalmar K, Victor JD, Baker K, Gerber M, Fritz B, Eisenberg B, O'Connor J, Kobylarz EJ, Farris S, Machado A, McCagg C, Plum F, Fins JJ, Rezai AR, 2007. Behavioural improvements with thalamic stimulation after severe traumatic brain injury. Nature 448, 600–603. doi: 10.1038/nature06041. [PubMed: 17671503]

Schroter MS, Spoormaker VI, Schorer A, Wohlschlager A, Czisch M, Kochs EF, Zimmer C, Hemmer B, Schneider G, Jordan D, Ilg R, 2012. Spatiotemporal reconfiguration of large-scale brain functional networks during propofol-induced loss of consciousness. J. Neurosci 32, 12832–12840. doi: 10.1523/jneurosci.6046-11.2012. [PubMed: 22973006]

Sepúlveda PO, Tapia LF, Monsalves S, 2019. Neural inertia and differences between loss of and recovery from consciousness during total intravenous anaesthesia: a narrative review. Anaesthesia 74, 801–809. doi: 10.1111/anae.14609. [PubMed: 30835820]

Shafer S, 1996. STANPUMP User's Manual. Stanford University, Stanford, CA Source http://opentci.org/code/stanpump.

Solt K, Van Dort CJ, Chemali JJ, Taylor NE, Kenny JD, Brown EN, 2014. Electrical stimulation of the ventral tegmental area induces reanimation from general anesthesia. Anesthesiology 121, 311–319. doi: 10.1097/ALN.0000000000000117. [PubMed: 24398816]

Song AH, Kucyi A, Napadow V, Brown EN, Loggia ML, Akeju O, 2017. Pharmacological modulation of noradrenergic arousal circuitry disrupts functional connectivity of the locus ceruleus in humans. J. Neurosci 37, 6938–6945. doi: 10.1523/JNEUROSCI.0446-17.2017. [PubMed: 28626012]

Steyn-Ross ML, Steyn-Ross DA, Sleigh JW, 2004. Modelling general anaesthesia as a first-order phase transition in the cortex. Prog. Biophys. Mol. Biol 85, 369–385. doi: 10.1016/j.pbiomolbio.2004.02.001. [PubMed: 15142753]

Su CW, Zheng L, Li YJ, Zhou HJ, Wang J, Huang ZG, Lai YC, 2020. Hysteresis in anesthesia and recovery: experimental observation and dynamical mechanism. Phys. Rev. Res 2, 023289. doi: 10.1103/physrevresearch.2.023289.

Supp GG, Siegel M, Hipp JF, Engel AK, 2011. Cortical hypersynchrony predicts breakdown of sensory processing during loss of consciousness. Curr. Biol 21, 1988–1993. doi: 10.1016/j.cub.2011.10.017. [PubMed: 22100063]

Suzuki M, Larkum ME, 2020. General anesthesia decouples cortical pyramidal neurons. Cell 180. doi: 10.1016/j.cell.2020.01.024,666-676.e13.

Tagliazucchi E, Chialvo DR, Siniatchkin M, Brichant JF, Laureys S, Amico E, Brichant JF, Bonhomme V, Noirhomme Q, Laufs H, Laureys S, 2016. Large-scale signatures of unconsciousness are consistent with a departure from critical dynamics. J. R. Soc. Interface 13, 1–34. doi: 10.1098/rsif.2015.1027.

Tanabe S, Huang Z, Zhang Jun, Chen Y, Fogel S, Doyon J, Wu J, Xu J, Zhang Jianfeng, Qin P, Wu X, Mao Y, Mashour GA, Hudetz AG, Northoff G, 2020. Altered global brain signal during physiologic, pharmacologic, and pathologic states of unconsciousness in humans and rats. Anesthesiology 132, 1392–1406. doi: 10.1097/aln.0000000000003197. [PubMed: 32205548]

Tarnal V, Vlisides PE, Mashour GA, 2016. The neurobiology of anesthetic emergence. J. Neurosurg. Anesthesiol 28, 250–255. doi: 10.1097/ANA.0000000000000212. [PubMed: 26274626]

Taylor NE, Van Dort CJ, Kenny JD, Pei J, Guidera JA, Vlasov KY, Lee JT, Boyden ES, Brown EN, Solt K, 2016. Optogenetic activation of Dopamine neurons in the ventral tegmental area induces reanimation from general anesthesia. Proc. Natl. Acad. Sci. USA 113, 12826–12831. doi: 10.1073/pnas.1614340113. [PubMed: 27791160]

Tzourio-Mazoyer N, Landeau B, Papathanassiou D, Crivello F, Etard O, Delcroix N, Mazoyer B, Joliot M, 2002. Automated anatomical labeling of activations in SPM using a macroscopic anatomical parcellation of the MNI MRI single-subject brain. Neuroimage 15, 273–289. doi: 10.1006/nimg.2001.0978. [PubMed: 11771995]

Veselis RA, 2001. Anesthesia - a descent or a jump into the depths? Conscious. Cogn 10, 230–235. doi: 10.1006/ccog.2001.0513. [PubMed: 11414717]

Voss LJ, Brock M, Carlsson C, Steyn-Ross A, Steyn-Ross M, Sleigh JW, 2012. Investigating paradoxical hysteresis effects in the mouse neocortical slice model. Eur. J. Pharmacol 675, 26–31. doi: 10.1016/j.ejphar.2011.11.045. [PubMed: 22166374]

Wang TX, Xiong B, Xu W, Wei HH, Qu WM, Hong ZY, Huang ZL, 2019. Activation of parabrachial nucleus glutamatergic neurons accelerates reanimation from sevoflurane anesthesia in mice. Anesthesiology 130, 106–118. doi: 10.1097/ALN.0000000000002475. [PubMed: 30325744]

Warnaby CE, Seretny M, Mhuircheartaigh RN, Rogers R, Jbabdi S, Sleigh J, Tracey I, 2016. Anesthesia-induced suppression of human dorsal anterior insula responsivity at loss of volitional behavioral response. Anesthesiology 124, 766–778. doi: 10.1097/ALN.0000000000001027. [PubMed: 26808631]

Warnaby CE, Sleigh JW, Hight D, Jbabdi S, Tracey I, 2017. Investigation of slow-wave activity saturation during surgical anesthesia reveals a signature of neural inertia in humans. Anesthesiology 127, 645–657. doi: 10.1097/ALN.0000000000001759. [PubMed: 28665814]

White NS, Alkire MT, 2003. Impaired thalamocortical connectivity in humans during general-anesthetic-induced unconsciousness. Neuroimage 19, 402–411. doi: 10.1016/S1053-8119(03)00103-4. [PubMed: 12814589]

Zhang Z, Ferretti V, Güntan I, Moro A, Steinberg EA, Ye Z, Zecharia AY, Yu X, Vyssotski AL, Brickley SG, Yustos R, Pillidge ZE, Harding EC, Wisden W, Franks NP, 2015. Neuronal ensembles sufficient for recovery sleep and the sedative actions of α 2 adrenergic agonists. Nat. Neurosci 18, 553–561. doi: 10.1038/nn.3957. [PubMed: 25706476]

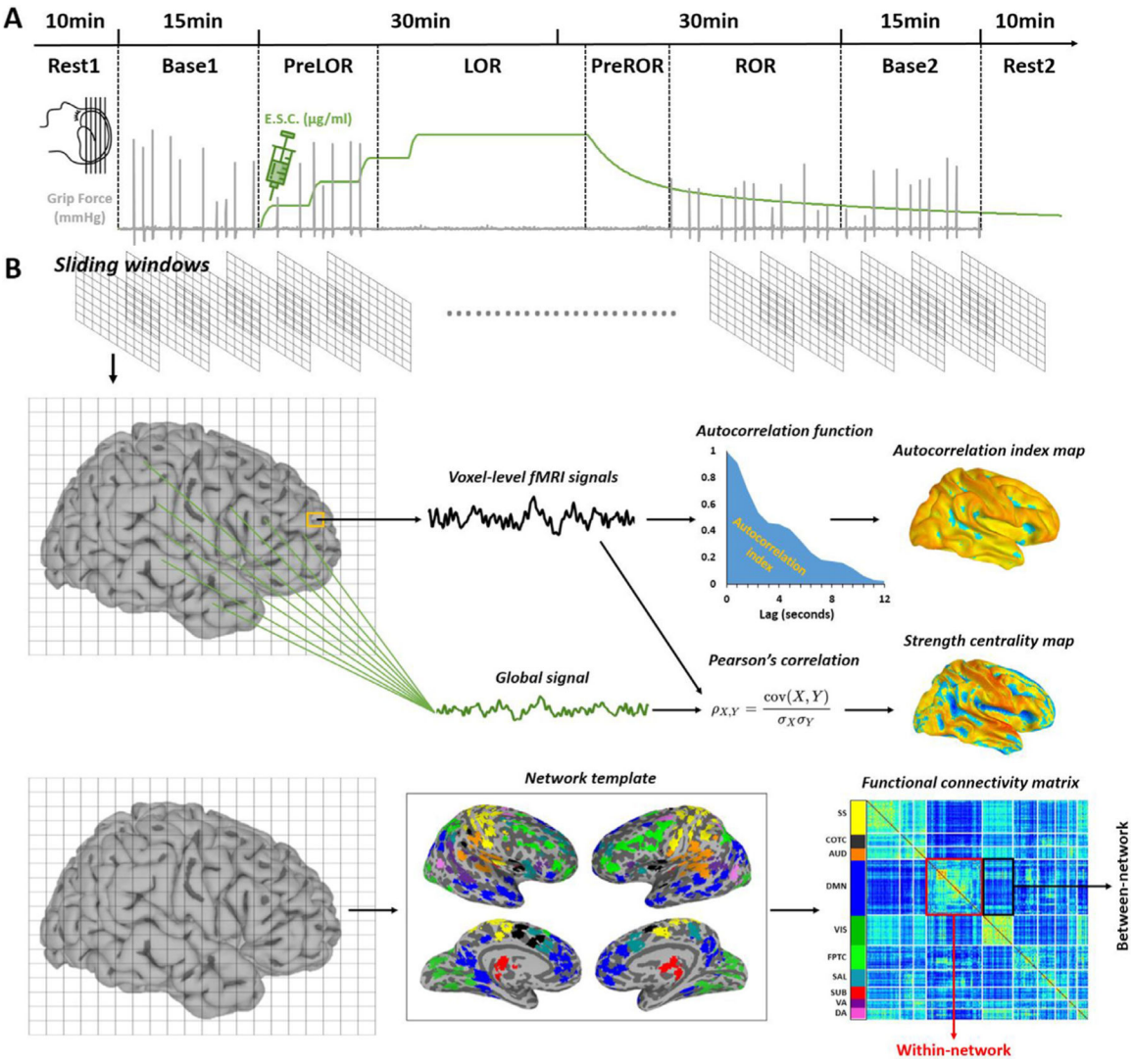

Fig. 1. Experimental design and fMRI measures.

(A) Healthy volunteers were studied using fMRI before, during, and after intravenous propofol infusion. The infusion rate was adjusted to achieve stepwise increasing target effect-site concentrations. Behavioral responsiveness was assessed by motor response, which defined the periods during which a participant retained responsiveness (PreLOR), loss of responsiveness (LOR) before spontaneous emergence, prior to recovery of responsiveness during emergence (PreROR), and recovery of responsiveness (ROR). Two 10 min resting-state baseline and two 15 min task baseline recordings were done before (Rest1 and Base1) and after (Base2 and Rest2) propofol infusion. **(B)** A sliding window approach (window size = 2 min; time step = 20 s) was used to analyze the time courses of fMRI-derived quantities. The timescale of fMRI signals was estimated for each voxel as the temporal autocorrelation decay, quantified as the area under the curve (AUC) of the autocorrelation function from 0.8 to 12 s. Voxel-wise strength centrality was defined by calculating the Pearson's correlation coefficient between a given voxel's signal and the global (gray matter average) signal. Within- or between-network functional connectivity was derived by computing the average

of the triangular or rectangle zones of the functional connectivity matrix corresponding to a given network (within-network) or a pair of networks (between-network). The functional connectivity matrix was generated by calculating the Pearson's correlation coefficient of the time courses between each pair of functional areas based on a pre-defined network template. The networks include subcortical (SUB), dorsal attention (DA), ventral attention (VA), default mode (DMN), fronto-parietal task control (FPTC), cingulo-opercular task control (COTC), salience (SAL), sensory/somatomotor (SS), auditory (AUD), and visual networks (VIS).

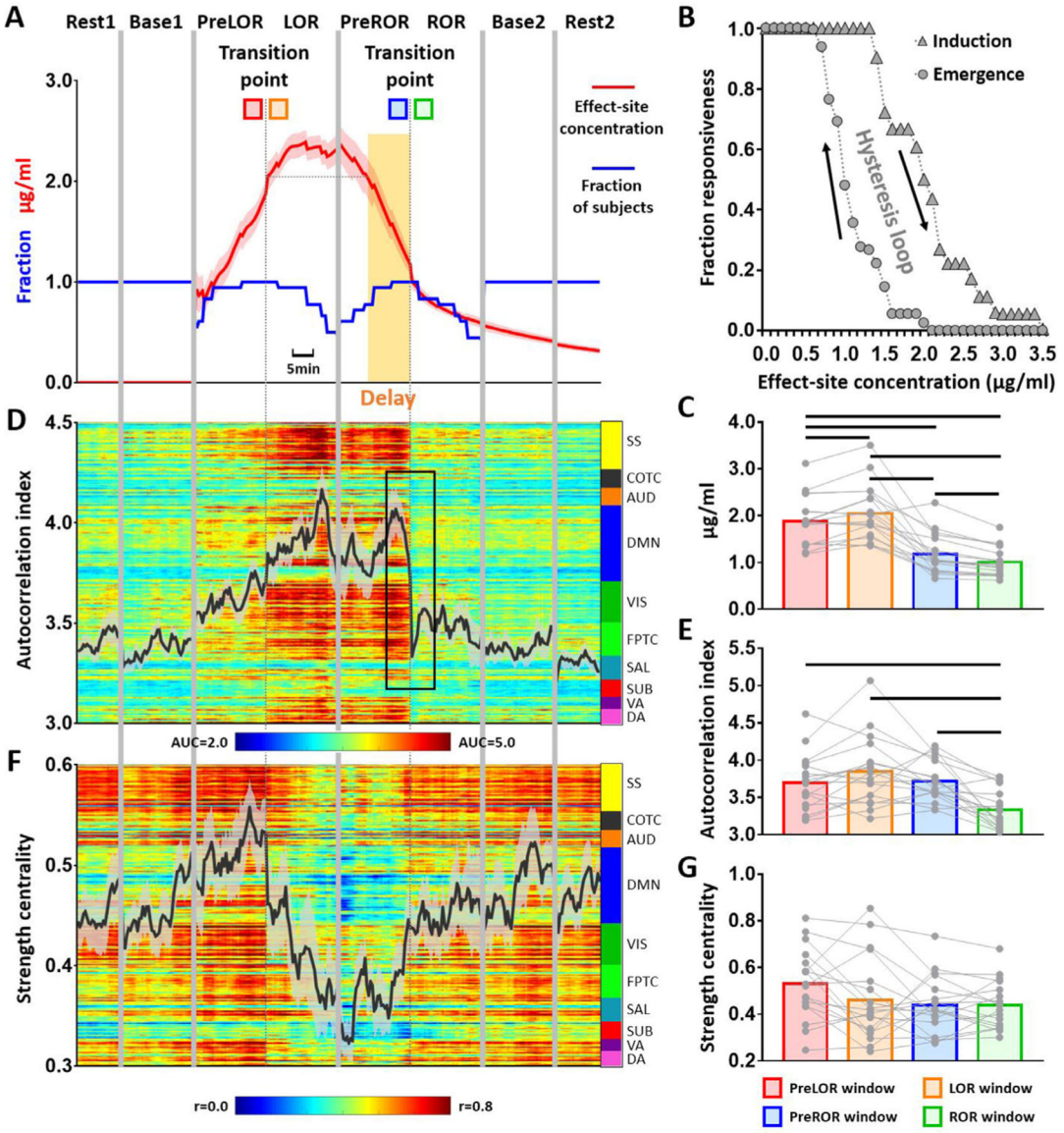

Fig. 2. Induction-emergence hysteresis and global changes of brain activity.

(A) Group average of propofol effect-site concentration (ESC). Given the data length of PreLOR, LOR, PreROR and ROR varied across participants, the transition points of LOR and ROR were used as two reference time points in order to align all participants' data within the same timeline. The sliding window was moving forward and backward centered at the reference time points, with a maximum data length of 15 min in each time direction. The transition to ROR occurred at a lower ESC than during the transition to LOR. The delayed period in the recovery of behavioral responsiveness with respect to the same level of anesthetic dose at LOR is indicated by a yellow shaded area. **(B)** A hysteresis loop is shown by plotting the fraction of responsiveness (across subjects) vs. estimated propofol effect-site concentration. The area between the curves of induction and emergence represents a resistance to change in the state of consciousness. **(D)** Time course of global (gray matter average) autocorrelation index at the group-level. **(F)** Time course of global strength

centrality at the group-level. **(C, E, G)** Measurements taken before and after LOR and ROR were statistically compared from 120 s data windows preceding (PreLOR and PreROR) and following (LOR and ROR) the state transition points by two-tailed paired-sample t-tests (df = 17). Black lines on the bars indicate statistical significance at FDR-corrected $\alpha < 0.05$. Shaded areas in the time courses indicate ±SEM.

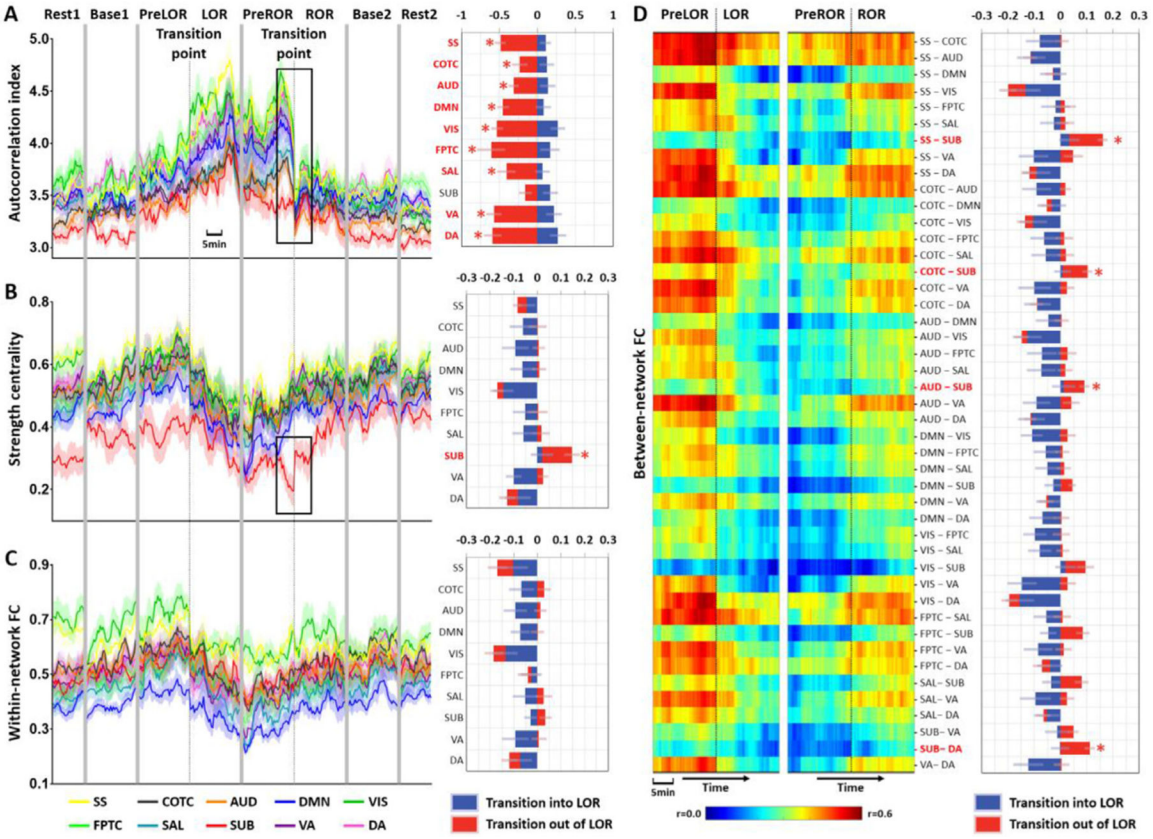

Fig. 3. Network changes of brain activity during state transitions.

(A) Left panel: time courses of autocorrelation index in different networks at the group-level; right panel: measurements taken before and after LOR and ROR were statistically compared from 120 s data windows preceding (PreLOR and PreROR) and following (LOR and ROR) the state transition points by two-tailed paired-sample t-tests (df = 17). Blue bars represent the differences for LOR vs. PreLOR, namely transition in to LOR. Red bars represent the differences for ROR vs. PreROR, namely transition out of LOR. **(B)** Time courses (left) and bar charts (right) for strength centrality in different networks at the group-level. **(C)** Time courses (left) and bar charts (right) for within-network functional connectivity at the group-level. **(D)** Time courses (left; heat maps) and bar charts (right) for between-network functional connectivity at the group-level. Asterisk (*) indicates statistical significance at FDR-corrected $\alpha < 0.05$. Shaded areas in the time courses indicate ± SEM. The networks include subcortical (SUB), dorsal attention (DA), ventral attention (VA), default mode (DMN), fronto-parietal task control (FPTC), cingulo-opercular task control (COTC), salience (SAL), sensory/somatomotor (SS), auditory (AUD), and visual networks (VIS).

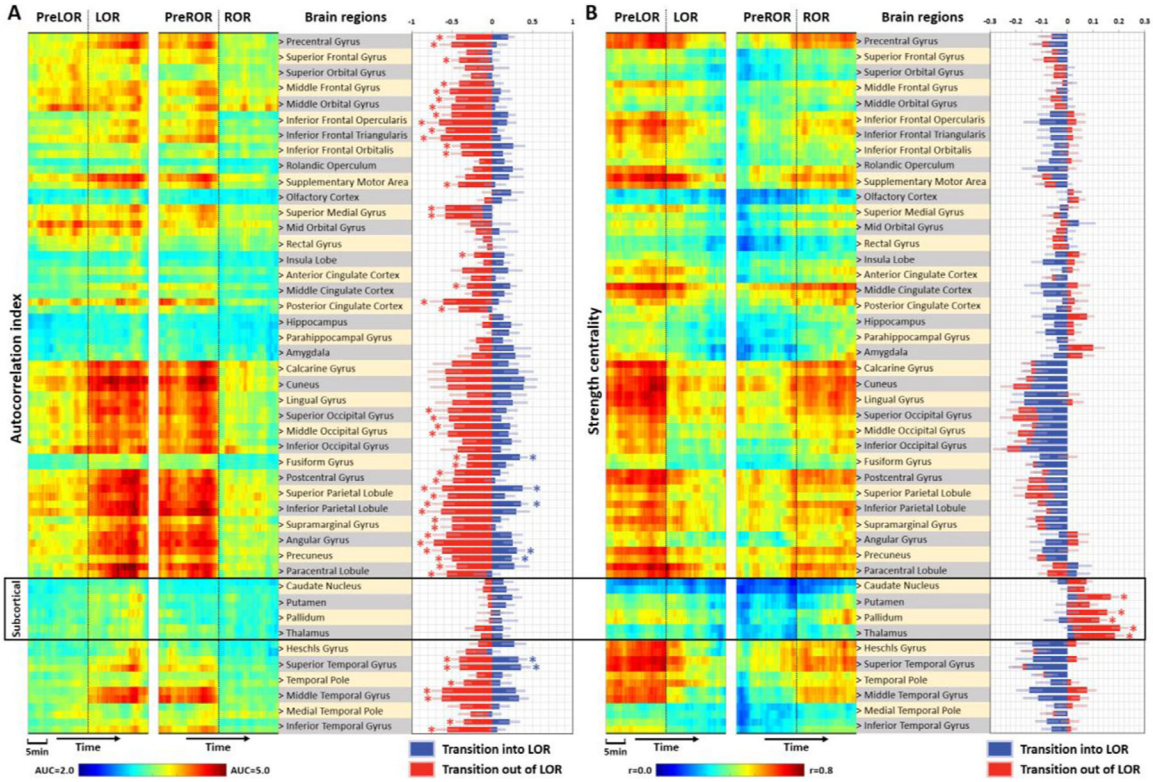

Fig. 4. Regional distribution of brain activity changes during state transitions.

(A) Left panel: time courses of autocorrelation index in pre-defined anatomical regions; middle panel: brain regions in the automated anatomical labeling (AAL) atlas (45 regions per hemisphere). A single brain region label corresponds to a pair of values from left (upper) and right (lower) hemispheres; right panel: blue bars represent the differences for LOR vs. PreLOR, namely transition in to LOR. Red bars represent the differences for ROR vs. PreROR, namely transition out of LOR. **(B)** Time courses and bar charts for strength centrality in different brain regions at the group-level. Asterisk (*) indicates statistical significance at FDR-corrected $\alpha < 0.05$.

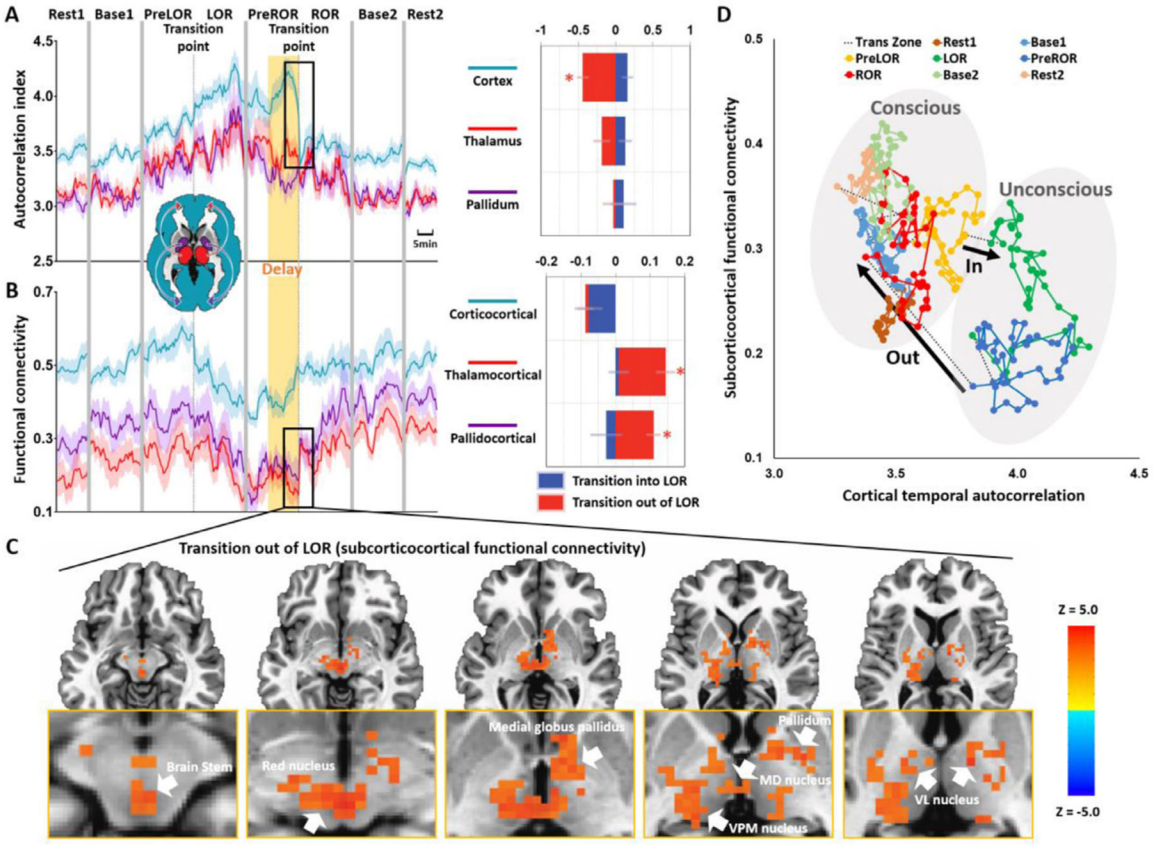

Fig. 5. Temporal trajectory of functional connectivity and temporal autocorrelation during state transitions.

(A) Time courses of autocorrelation index in the cortex, thalamus and pallidum at the group-level. **(B)** Time courses of corticocortical, thalamocortical and pallidocortical functional connectivity at the group-level. Asterisk (*) indicates statistical significance at FDR-corrected $\alpha < 0.05$. Shaded areas in the time courses indicate ± SEM. **(C)** Whole-brain functional connectivity was calculated by using the average fMRI time series across the entire cortex as a regressor. Voxel-wise paired sample t-tests (two-sided) between PreROR window and ROR window were performed at the group-level. The resulting z-map was thresholded at the cluster level $\alpha < 0.05$. The abrupt boost of subcorticocortical functional connectivity during regaining consciousness included the brain stem, red nucleus, medial globus pallidus, pallidum, medial dorsal (MD) nucleus, ventral posteromedial (VPM) nucleus and ventral lateral (VL) nucleus. **(D)** The trajectory of subcorticocortical functional connectivity (average of thalamocortical and pallidocortical functional connectivity) was plotted as a function of the cortical signal's temporal autocorrelation.